INFERRING INTERWELL CONNECTIVITY FROM INJECTION AND PRODUCTION DATA USING FREQUENCY DOMAIN ANALYSIS

A Thesis

by

AYSE NAZLI DEMIROREN

Submitted to the Office of Graduate Studies of
Texas A&M University
in partial fulfillment of the requirements for the degree of

MASTER OF SCIENCE

May 2007

Major Subject: Petroleum Engineering

INFERRING INTERWELL CONNECTIVITY FROM INJECTION AND PRODUCTION DATA USING FREQUENCY DOMAIN ANALYSIS

A Thesis

by

AYSE NAZLI DEMIROREN

Submitted to the Office of Graduate Studies of
Texas A&M University
in partial fulfillment of the requirements for the degree of

MASTER OF SCIENCE

Approved by:

Chair of Committee,	Jerry L. Jensen
Committee Members,	Thomas A. Blasingame
	Richard L. Gibson
Head of Department,	Stephen A. Holditch

May 2007

Major Subject: Petroleum Engineering

ABSTRACT

Inferring Interwell Connectivity from Injection and Production Data

Using Frequency Domain Analysis. (May 2007)

Ayse Nazli Demiroren,

B.S., Istanbul Technical University

Chair of Advisory Committee: Dr. Jerry L. Jensen

This project estimates interwell connectivity, a characteristic that is crucial to determine reservoir continuity while developing a waterflooding project. It tests the combination of Fourier transforms (FT's) of the flow rate data and analytical solutions from analog electrical circuits to infer the inverse diffusivity coefficient (IDC). I solved the transmission line equation analytically for 0D, 1D, and 2D resistance/capacitance (RC) network models and used those solutions to compare with the flow rate FT's to determine the diffusivity parameters. I used the analogy between the electrical response of RC networks and the fluid response of permeable reservoirs on the basis of the similarities in the governing equations.

I conclude that the analogy works accurately in simple reservoirs, where the assumptions of an analytical solution are met, *i.e.* single-phase fluid and a homogeneous system. For two-phase liquid cases, I determined that the analogy remains applicable because we still could produce accurate interwell connectivity information. When I investigated cases with dissolved-gas production around the wellbore, however, the analogy broke down and the results were not as good as the liquid systems.

ACKNOWLEDGEMENTS

I would sincerely like to express my gratitude to Dr. Jerry L. Jensen for his patience, help and guidance to complete this research project; Dr. Larry Lake for his constructive comments throughout the interwell connectivity progress meetings, and Dr. Jim Ji for enlightening me on digital signal processing. I would like to thank to Dr. Thomas A. Blasingame and Dr. Richard L. Gibson for serving as members of my advisory committee.

I would like to express my appreciation to my officemates for their help, support and fun times in our room 621 at Richardson Building: Danial Kaviani and his wife Sahar Ghanbarzadeh Gargary, Weiqiang Li, Fuyong Yan, Eser Akoz. I should acknowledge Dilhan Ilk's efforts, who had a huge portion in making my final decision to come to College Station pursuing my MS degree. He offered his friendship and incredible help during a certain period of my life in College Station.

My dear friend Burak Pak, whom I met during his visiting position at Texas A&M University, has been the most memorable member of my family in the United States, which, I hope, will last forever anywhere around the world.

Finally, I would like to thank my mother, my spiritual mentor, my father, in Istanbul and my little family including my lovely grandparents, my brother-like cousins and their parents, and my friends (KPG). They have never left me alone here and have always been with me anytime.

TABLE OF CONTENTS

LIST OF FIGURES

FIGURE Page

FIGURE Page

LIST OF TABLES

CHAPTER I

INTRODUCTION

1.1 Introduction

The main objective of this work is to develop a proof of concept to infer interwell connectivity between an injector, and a producer in a waterflooded field. This study is performed to determine if certain deviations from the assumed conditions can be tolerated by the method while still producing an accurate estimate of interwell connectivity.

This chapter includes the overall objectives of the study and the literature review in previous interwell connectivity studies, use of sinusoidal rates in reservoir characterization, use of electrical analogs in reservoir engineering and the mathematical background in FT's.

1.2. Research Objectives

The overall objectives of this work are:

- To apply a method using the FT's of the flow rate data.
- Exploit the correspondence of fluid flow with electrical RC network models to estimate the diffusivity parameters.
- To validate the use of this technique by applying it to the hypothetical cases.
- To examine the effects of gas around the wellbore that might cause inconsistency in interwell connectivity analyses by using the proposed technique.
- To list the conditions under which this concept is applicable.

This thesis follows the style and format of the *SPE Journal*.

1.3. Statement of the Problem

As noted by Muskat (1949), an electrical analyzer is a powerful tool to analyze water-drive reservoirs when the reservoir itself is not of simple geometry or uniform physical properties. Keeping this in mind, the basic idea here in our study is to assume that the reservoir system is equivalent to a resistance-capacitance network, where the fluid flow in a porous media is equivalent to the flow of an electric current in a circuit.

Fluid flow can only occur when pore spaces in the reservoir rock are connected. In the same way, electricity can only flow if conductive materials are connected to each other, forming a circuit for electricity to follow. This similarity is expressed by the mathematical equations describing the flow. The hydraulic and electrical conductivities are related because of the similarity between the differential equations describing each process. More specifically, the reason why we use the analogy between reservoir and RC network is that the capacitance placed in an RC circuit is capable of storing electrical energy in itself; similarly, the reservoir is also a permeable rock that stores mechanical energy due its compressibility.

Physically, for 0D (tank) models, the dissipation of the electrical current or the fluid wave depends on the change of voltage or pressure in time with regardless of dimensions of the model. The lumped values of the parameters through the reservoir or the circuit are used in the calculations. Therefore, the interwell connectivity information estimated from those models can not reflect the heterogeneity of the displacement processes. On the other hand, in 1D and 2D dimensional models, the length of the model, the interwell distance and the spatial distributions of the parameters, *i.e* R, C, ϕ, k …, can be incorporated into the calculations. Hence, those models offer more sophisticated solutions to predict the interwell diffusivity for a displacement process.

Mathematically, the similarity of the governing equations of fluid and electrical flow also provide us an opportunity to express the analogy between permeable reservoir rocks and conductive RC systems.

RC network analogs were introduced to the literature by Bruce (1943) to simulate the unsteady-state performance of undersaturated oil reservoirs under water drive. In that study, he used the capacitance term in the RC network to model the storage term in the reservoir. He used the storage equation (Eq. 1.1). Physically, he assumed the reservoir as a tank model where mass of fluid flowing in less the mass flowing out is equal to the accumulation term from material balance and depends on the change in pressure with time regardless of what the reservoir dimensions are. Accordingly, he showed the storage equation in electrical flow (Eq. 1.2) as analogous to the fluid flow. In these equations, he expressed the accumulation by the product of the pore volume and the total compressibility factor in a reservoir and by a capacitance term in an analog RC device. Thereby, he constructed a link analytically between the coefficients of the time derivatives in those equations. However, the resistance that is analogous to the transmissibility term in a reservoir is ignored in his models since the model that he used in his study is only a tank model, in other words a dimensions-free network.

$$q_1 - q_2 = V_p c_t \frac{dp}{dt}. \quad \text{.....(1.1)}$$

$$i_1 - i_2 = C_E \frac{dv}{dt}. \quad \text{.....(1.2)}$$

Where

C_E	=	Capacitance, μfarads
V_p	=	Pore volume, bbl
c_t	=	Total compressibility, 1/psi
q_1	=	Flow rate in, bbl/day
q_2	=	Flow rate out, bbl/day
p	=	Pressure, psi
t	=	Time, day
i_1	=	Current in, μA
i_2	=	Current out, μA
v	=	Voltage, volts

Alternatively, we introduce an analogy between fluid flow and electrical flow that has the ability of incorporating dimensional models into the study to identify more complex reservoirs by analog RC devices. Our initiative to apply sinusoidal rates to the injecting well comes from the electrical systems in which it is easy and common to use sinusoidal excitations to identify a linear system. Furthermore, the similarity of the governing equations lets us perform an analogy to determine interwell diffusivity. Therefore, we use Eq. 1.3 that is the fluid flow diffusivity equation in petroleum engineering studies (e.g., Lee, 2003, p.4) and Eq. 1.4 that is the transmission line equation for the voltage distribution in communications engineering (Everitt, 1956, p.303). Mathematically, imposing the same boundary conditions on those two equations results in similar distributions for pressure and voltage. Then, we can easily show that the pressure difference in a reservoir between two locations is equivalent to the difference in voltage in an RC network between two terminals.

$$\frac{\partial^2 p}{\partial z^2} = \frac{\phi \mu c_t}{k} \frac{\partial p}{\partial t}. \quad \text{.....(1.3)}$$

$$\frac{\partial^2 v}{\partial z^2} = RC \frac{\partial v}{\partial t}. \quad \text{.....(1.4)}$$

Where

z = Point in space, ft
ϕ = Porosity, d.less
μ = Viscosity, cp
k = Permeability, md
v = Voltage, volts
R = Resistance, ohms
C = Capacitance, farads

Since we can solve pressure and voltage differences between two ends analytically for dimensional models from Eqs 1.3 and 1.4, we can also incorporate the resistance term of an RC network, which was ignored earlier by Bruce. We can construct an alternative analogy between fluid and electrical flow by using the

information from both capacitance and resistance. We aim to use RC analog networks not only for a tank model, but also for 1D and 2D models in our study, then we can consider the interwell distance and the reservoir geometry and the spatial distribution of the diffusivity parameters in estimation of interwell connectivity. When we compare Eqs. 1.3 and 1.4, the analogy is exact for 1D and 2D models as we give in the following form:

$$\frac{\phi\mu c_t}{k} = RC \; . \qquad (1.5)$$

The units of both expressions in Eq. 1.5 are in T/L^2. Hereinafter, we name the left hand side of Eq.1.5 the inverse diffusivity coefficient (IDC).

The important thing for the dimensionless 0D RC model is that the voltage difference in the circuit is not a function of the length of the circuit; therefore, the transmissibility is not included in the analogy between the reservoir and the analog RC device. There is no resistance in the 0D system because it only stores material (charge or fluid). There has to be flow of charge or fluid for resistance (energy loss) to come into play:

$$V_p c_t = C \; . \qquad (1.6)$$

In electrical engineering, as we mentioned it is a very common procedure to apply a sinusoidal input to an RC network and to measure the system output at each frequency. The transfer function, *H(f)*, which is the output to input ratio of sinusoidal excitations can be calculated and plotted against frequency. This plot can be used to show how much of the input is being transferred to the output as the frequency changes. Likewise theoretically, we can apply this simple procedure to the reservoir assuming the injection rate data as the input and the production rate data as the output. In fluid flow; however, it is not simple to distinguish the frequency components of the rate distributions in the time domain. Therefore, we use FT to decompose the flow rate into its harmonic components. This way, it is also possible to calculate the transfer function (TF) of a reservoir as in Eq. 1.7 and plot it in the frequency spectrum.

$$H(f) = \frac{Y(f)}{X(f)} . \quad \text{.....(1.7)}$$

Where

Y(f) = FT of the production rate

X(f) = FT of the injection rate

H(f) = Reservoir transfer function (RTF)

Fourier analysis is named after Jean Baptiste Fourier, who showed that any periodic function can be represented as the sum of sinusoids with integrally related frequencies. The purpose of those analyses is to express a given arbitrary function, as a linear combination of a set of harmonic sine and cosine basis functions (Harman, 2000). The Fourier series approximates a function *f(t)* by using the following equation:

$$f(t) \approx \frac{a_0}{2} + \sum_{n=1}^{N} \left[a_n Cos(nt) + b_n Sin(nt) \right] = s_N(t) . \quad \text{.....(1.8)}$$

Where $s_N(t)$ is the Fourier approximation to the function *f(t)* obtained by using a trigonometric polynomial of degree *N* assuming *f(t)* is continuous on the interval [-π, π]. The constant term a_0 and the coefficients a_n and b_n in Eq. 1.8 can be computed by the following formulas for *n*=1,2…*N*.

$$a_0 = \frac{1}{\pi} \int_{-\pi}^{\pi} f(t)dt . \quad \text{.....(1.9)}$$

$$a_n = \frac{1}{\pi} \int_{-\pi}^{\pi} f(t)Cos(nt)dt . \quad \text{.....(1.10)}$$

$$b_n = \frac{1}{\pi} \int_{-\pi}^{\pi} f(t)Sin(nt)dt . \quad \text{.....(1.11)}$$

The discrete Fourier transform (DFT) of the transfer function, *H(f)*, produces a complex number that consists of a real part and an imaginary part. Those parts are used to calculate the magnitude and the phase of the transfer function. In theory, when a sinusoid enters a linear system, the output is also a sinusoid at exactly the same frequency as the input. Only the amplitude and phase can change. So, systems

can be represented by how they modify the amplitude and phase of the cosine waves. Therefore, the frequency domain representation of the transfer function is possible by the polar notation of the magnitude shown in the following equation:

$$\left|H(f)\right| = \sqrt{\left|H_r(f)\right|^2 + \left|H_i(f)\right|^2} \quad \text{.....(1.12)}$$

The magnitude gives information about the change in the amplitude of the input whereas the phase is informative about the phase shifts of the input.

In this study, we apply a method that requires us to investigate the degree of attenuation in the magnitude to infer the connectivity information; therefore, we use only the magnitude of the DFT of the injection and the production rates. The phase shift that we exclude tells us more about time lags that occur because of various reasons of reservoir heterogeneity.

We explain the basics of Fourier series more in Appendix A.

In this study, we compute FT's of the flow rate data in Matlab, which uses the fast Fourier transform algorithm (FFT). In **Fig. 1.1a**, we define a raw signal, *f(t)*, in the time domain as the following equation: $Cos(2\pi(0.125t)+Cos(2\pi(0.05t))$. In **Fig. 1.1b**, we represent the FT of the raw signal after we compute it in Matlab. The frequency components of that signal in the spectrum are found to be 0.05 Hz and 0.125 Hz, respectively. Our purpose to demonstrate those figures is to show that we apply FT to obtain further information, which might be hidden in its frequency content, from the signal that is not readily apparent in the raw signal.

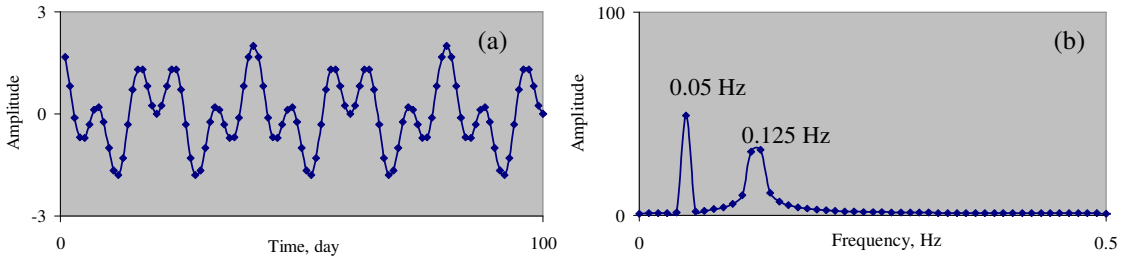

Figure 1.1—Representation of a given sinusoid in the time domain (a) and in the frequency domain (b).

We can recognize sinusoidal functions easily in the frequency spectrum, as we experience in the previous example. In the scope of this project, we also analyze random flow rate data as well as the sinusoidal rate data because the field data can not practically be periodic to carry out the FT and to do the spectral analysis in the frequency domain. However, the application of the random data produces some disadvantages throughout the spectral analyses, which we mention in Chapter II.

In the circuit analysis, *H(f)*, which is the transfer function, is analyzed to determine the value of *RC* coefficient. In a similar way, we analyze RTF to evaluate IDC, $\phi\mu c_t / k$ for dimensional models; $V_p c_t$ for 0D models. Then, we can use those coefficients to determine the reservoir connectivity.

To determine IDC, we use analytical solutions of Eq. 1.4. We solve the transmission line equation analytically in three ways:

- 0D RC Network Model: This is the storage equation in Eq. 1.1 where the dimensions of a circuit are reduced to 0 dimensions; therefore, the analogy is reduced to only capacitance term in the circuit. This model is analogous to the material balance tank model upon which Bruce also based his study in 1943. 0D model is a tank model that requires only the lumped values of the parameters; therefore, it lacks the resistance, which connects multiple blocks of reservoir or circuit, and spatial variations.

- 1D RC Network Model: It is the solution to a 1D voltage distribution in an RC network; therefore, it uses the resistance as well as the capacitance in the circuit while identifying the fluid flow. It designates the fluid flow in a very narrow reservoir where flow is restricted to one direction. This may be a channel, a fracture or some other narrow conduit of flow.

- 2D RC Network Model: It is the solution to a 2D voltage distribution in a radial system and provides a more sophisticated solution to the interwell connectivity problem. It describes

the fluid flow in a very large reservoir where drainage area is large enough for a multi-dimensional flow.

We provide more details on analog RC network models, their analytical solutions and frequency domain representations in Chapter II.

In this proposed work, the main goals are to compare the transfer functions of RC network models with those of flow rate data obtained from reservoir simulation to determine which network model behaves most similarly to the reservoir flow, and to investigate whether multi-phase production in the reservoir affect the similarity.

To achieve this, RTF's are compared with the three RC transfer functions (RCTF), which we produce from the analytical solutions. We performed the comparisons between RCTF and RTF in the frequency domain. We selected the analytical solution that fits the RTF curve best as the solution that represents the reservoir behavior. Eventually, assigning the coefficient of the best representative analytical solution, which is the RC network coefficient, to the diffusivity parameters yields the interwell connectivity information.

We use the analogies between the coefficients of the RC networks and the diffusivity parameters, Eqs. 1.5 and 1.6, as the basis of this study to interwell connectivity. Basically, we use reservoir parameters to calculate the RC network coefficient for a particular reservoir model. The reservoir model, of which its RTF matches its corresponding RCTF, approves the analogy under the given assumptions between the fluid flow and the electrical flow successfully.

In case of not being able to match none of the RCTF under exact reservoir parameters, we adjust the RC network coefficient to match the RTF. Then, we assign the modified coefficient back to the diffusivity parameters to predict a new range of ϕ / k .

Ultimately, we evaluate the interwell connectivity in terms of ϕ / k letting us make predictions about the range of the least predictable parameter in reservoir characterization that is the permeability. Since

porosity is mostly available from well logs and core data, this study offers an alternative way to estimate a range of permeability.

1.4 Literature Review

1.4.1 Interwell Connectivity Studies

There have been various studies that have attempted to resolve the uncertainty in interwell connectivity and to quantify the degree of communication between wells in a reservoir. These methods include non-parametric statistics, wavelets, neural networks, and material balance tank models.

Heffer *et al.* (1995) developed a new method to test two main principles:

- The rate correlations between wells are generally good indicators of communication in a reservoir.
- The rate correlations between wells can be explained partially by geomechanical processes.

The method that they developed, couples the lateral direction of the fluid flow and the orientation of horizontal earth stresses. To predict the lateral communicaton between wells, they used the Spearman rank correlation coefficients between pairs of wells, each pair comprising one injector and one producer. The Spearman rank correlation is a very convenient non-parametric (distribution-free) statistic which is used as a measure of the strength of the associations between the injector and producer flow rate data. However, the correlations that were calculated gave spurious negative correlations and no systematic behavior of correlations with time lag was found. Therefore, the applications were conducted with no time lag. Eventually, the two principles mentioned above were validated by the applications and it was concluded that the coupled model provides a better understanding of the reservoir behavior to optimize the waterflooding planning.

Refunjol (1996) applied the Spearman rank correlation coefficient to the flow rates of injector/producer pairs composed of each injection well and all adjacent producers. As an extension to the current literature at that time, she investigated the effect of time lag between injectors and producers. Different time lags were used to find a maximum rank correlation coefficient for each possible injector – producer pair, so

that the maximum coefficient values of all injectors could be used to predict the preferential flow trend in the reservoir. Refunjol also found negative correlation coefficients which she explained by the influence of a third well. Most of the results for maximum rank correlation ranged from zero time lag to 6 months. However, some of the results had time lags up to 23 months, which is an extremely long period of time. Overall, her work could determine the general preferential flow trends and the interwell connectivity between well pairs successfully.

De Sant Anna'Pizarro (1999) also used the Spearman rank correlation coefficient between the well pairs. He aimed to test the validity of the non-parametric statistics method and to explain the reasons of the negative correlation coefficients that Refunjol obtained. He used numerical simulations and pointed out the advantages and limitations of using the Spearman rank correlation coefficient of the flow rate data in reservoir characterization. He proved that the method seemed to be more appropriate to indicate the potential flow barriers and permeability anisotropy. He also concluded that the Spearman rank correlation coefficient can increase if the injection rate is autocorrelated with time.

Jansen and Kelkar (1997) applied wavelet transforms to describe the interwell relationships, stating that the conventional cross correlation techniques tend to fail since the production data are non-stationary. Thus, they suggested that production data needed to be treated firstly by wavelet transform, so that it could be broken down into its frequency spectra, then the cross correlation between the pairs of wells could be performed. Then, the interwell relationships could be described more reliably. The significance of this study was its ability to break the flow rate data into its frequency components and still retain the time information so that time dependent cross correlation methods could also be applied. They also believed that another property of the wavelet transform, which is the ability of treating non-stationary data, played a very important role while capturing the dynamics of the well behavior better. In this work, more reliable correlations between well pairs were successfully obtained.

Panda and Chopra (1998) suggested a different, integrated approach other than the statistics-driven methods to estimate the well interactions. They applied an artificial neural network, where the

multivariate data set includes the flow rate data of the well pairs, as well as the petrophysical parameters and well locations. The neural network was trained by a data set and the results were used to determine the presence of reservoir heterogeneities and the permeability trends. Eventually, this method seemed to work more accurately than cross correlating the flow rate data visually; therefore, it could be more successful in management of a waterflooding project. However, this method had some limitations such as the lack of physical process representation in neural networks. That limited its use in numerical simulation. The authors stated that it required more research.

Soeriawinata and Kelkar (1999) also applied Spearman rank cross correlation by considering that the well pairs operating simultaneously cause both superposition and noise. The authors stated that the superposition of injectors has a significant effect on a producer's response, which could be either constructive or destructive interference. The method includes a trial and error approach which aims to select the best well pair that has the highest correlation coefficient. The study was applied to a hypothetical waterflooding project as well as to a real field. The authors stated that the injected water flowing outside the lease boundary and the noise due to the inaccuracy in measurements resulted in lower cross correlations in the real field case, as they expected. An important assumption was made during this study, which was that the cross correlation of the summation of the water injection rates to the liquid production rate would be higher than the cross correlation of each single injector. Eventually, it was noted that this method was very helpful to define the reservoir connectivity and easy to use for small operator and producer companies.

Albertoni and Lake (2002) introduced a technique to estimate the interwell connectivity based on a linear model by combining multivariate regression analysis with diffusivity filters that account for the time lags and the attenuation between the wells. The method allows a fieldwide analysis to be made, where all the wells can be analyzed at a single step. It offers two solutions covering the case when the fieldwide injection rate is different than the fieldwide liquid production rate and the case when the two are almost equal. The linear model weighting coefficients are shown to be independent of the injection and production rate data and depend solely on geology and relative position amongst the wells. The model

they created is free of the compressibility parameter; therefore, it does not include the capacitance effect and is a purely "resistive" model which is useful for determining the permeability trend. The method is validated on two different hypothetical fields and an application to a real field in Argentina. They tested the hypothetical models in anisotropic media through multi-layered reservoirs, reservoirs with a sealing fault or partially sealing faults, or with a channel. The applications of this method were restricted to only oil and water production; free gas production was not included in the calculations. The assumptions that were made throughout the work are no change in the number of wells, in BHP of the producers, in skin and well properties, in total compressibility factor, completion procedures, and in the effective permeabilities.

Al-Yousef *et al.* (2005) modified the technique introduced by Albertoni and Lake (2002) to describe the interwell connectivity based on fluctuations in production and injection rates. They extended the work by using a nonlinear model which includes a capacitance term that accounts for the system compressibility. They also used analog RC models which were based on a tank model and they used the productivity index as analogous to the capacitance term. The model determines two coefficients to better quantify the interwell connectivity. The first of these two coefficients is the weight that quantifies the connectivity and should depend on the geology and the relative position of wells. The second coefficient is the time constant which quantifies the degree of fluid storage between wells. The advantages of this method compared to the previous work are the applicability to the fields where the wells are frequently shut-in and the flow rates include primary production. This method also can incorporate the BHP values if available.

1.4.2 Studies Using Sinusoidal Rates in Reservoir Description

In reservoir characterization, sinusoidal rate application has been used for decades. It is attractive due to the periodic nature of the fluctuations, which makes the main signal easier to recognize among various types of noise in the reservoir. Sinusoids broaden the applicability of the analyses into frequency spectra, which enables us to use various tools such as the FT and wavelets. Eventually, the frequency representation of the sinusoidal data may provide more information to evaluate the reservoir behavior.

Johnson *et al.* (1966) developed a new method, named "pulse-testing" alternative to interference tests. The interference test is not practical due to the interruption of all field operations held during the test and the very long periods of time necessary to obtain a measurable pressure response with the conventional gauge at the responding well. The method of Johnson *et al*. is able to measure transmissibility and storage between a pulsing well and a responding well with the help of a more sensitive gauge than the conventional one. The advantage of pulse-testing is that imposing a series of pulses(cyclic disturbance) makes it easier to diagnose and distinguish the pressure response from noise at the responding well. The exponential integral solution to the diffusivity equation is used to describe the pulse-test pressure response. The response amplitude and the time lag obtained from the test results are used to calculate the average values for transmissibility and storage. In simple reservoirs, where the assumptions of the analytical solution are met, this method can provide quantitative values for reservoir parameters; on the other hand it provides qualitative information in heterogeneous and complex reservoirs. It is concluded that the response amplitude is dependent on well spacing, transmissibility, pulse interval and shut-in period as well as the rate of the pulse.

Kuo (1971) introduced analyses to determine reservoir properties from flow tests in one or more wells by imposing either sinusoidal or periodic multiple rates. He derived the pressure response equations based on the radial diffusivity equation and offered equations to calculate permeability values and the skin factor. In the case where a sinusoidal flow rate is imposed at either a single well or several wells, the pressure responses are calculated from the equations and the reservoir parameters are measured from the maximum response amplitude and the phase lag. On the other hand, in application of periodic multiple rates, formation parameters are calculated from the slope and intercept of a linear pressure response against time function. The result of that work is that if a sinusoidal flow rate is imposed to a well, the responding flow rate will be also periodic after the transients passed. This method is very similar to the conventional drawdown or multi rate flow tests; however, it differs in regulating the flow rates and interpreting the results. Those solutions are valid under homogenous, single-phase and slightly compressible reservoir conditions and have no advantages compared to the previous work by Johnson *et al.* (1966). However, in

heterogeneous reservoirs, plotting the amplitude ratio and phase shift against frequency provides a possibility of determining heterogeneities. Moreover, application of both single and multi-well tests enables flexibility to compare the solutions between wells and offer more accurate results.

Rosa and Horne (1991) developed an analytical solution to quantify the pressure response caused by cyclic flow rate variations in a heterogeneous reservoir with radial permeability variation assuming single-phase flow, slightly compressible fluid and isotropic porous medium properties. They applied the perturbation method for a qualitative analysis and to initiate the quantitative study. The method comes up with a useful formula that expresses the radius of cyclic influence in terms of the frequency of the cyclic flow rate. The radius of cyclic influence identifies the region of the reservoir that is influenced by the pressure response during a pulse test. This formula is used to design the pulse-test to yield the optimum result in estimating the permeability distribution. The results of this work on multi-composite radial reservoirs are very enlightening in terms of understanding the frequency dependent mechanisms in a reservoir. For instance, it is concluded that pressure responses caused by the flow disturbances are sensitive to the permeabilities of different regions. It is shown that the higher the frequency, the larger is the region of influence between the well pairs at multi-well flow tests. The idea behind that is the increasing frequency enhances the contribution from the permeabilities near the pulsing well because the high frequencies do not deeply go into the reservoir, they just go to the region near the pulsing well.

Hollaender, *et al.* (2002) proposed that harmonic testing can be used to determine the same reservoir parameters as conventional testing. However, there are some limitations and also some advantages in using flow rate data which are generated periodically during well tests. These issues are explained by several practical applications. In some applications, Fourier analysis is used to determine the amplitude and the phase shift of the sinusoidal variation of the flow rate to use it in the interpretation of the well test. It is concluded that it takes more time to run harmonic testing to obtain the same amount of information as conventional testing. The good point is that it does not require interrupting the production. These tests are less influenced by the noise and the potential noise can be averaged effectively. Since there is not a very high signal-to noise ratio, it enables to operate with small rate changes, which minimizes rate dependent

non-Darcy effects. The study is based on single-phase liquid production. The gas well harmonic testing is said to be significantly more complex and is not included in this work.

A major concern in reservoir connectivity has been to establish the most reliable and consistent reservoir behavior under certain assumptions. Generally, this is achieved by trying to describe the response of reservoir to a certain known stimulus through various methods. As mentioned, the more recognizable a stimulus applied upon the reservoir is, the better and closer reservoir identification can possibly be made.

Among all these works, a general concept that captures the reservoir behavior by broadening the applicable methods into frequency domain by particularly using the electrical analogs of the reservoir will be very useful and enlightening.

1.4.3 Studies Using Electrical Devices in Reservoir Identification

RC analog models, based on Bruce's methodology, were applied on 4 reservoir fields in Saudi Arabia in 1960s. The work performed by Wahl, *et al.* (1962) explains how a huge RC network that had 2501 capacitors and 4900 resistors was built to simulate the fluid flow in oil reservoirs. The field was divided into gridblocks to correspond to the mesh points in the RC model. The results of the analog model and the reservoir were compared in terms of field pressure and the graphs are presented in the work. The history match of the average field pressure in the reservoir provided very good results to model future predictions of reservoir performance.

1.4.4 Frequency Response Analysis

The information in signals is provided in two ways as in time and frequency domains. The simplest way to analyze the signal is in the time domain because each measured sample contains information that is interpretable without reference to any other sample and you know at what amplitude when the event takes place. On the other hand, the information provided by frequency domain is more indirect and it requires

relationship between many points in the signal. By taking advantage of the periodicity of the many things in the universe, information can be obtained in terms of frequency, phase and amplitude (Smith, 1999).

Systems are analyzed in the time domain by using convolution. A similar analysis can be done in the frequency domain. Using the FT, every input signal can be represented as a group of cosine waves, each with a specified amplitude and phase shift. The DFT (Discrete Fourier Transform) can be used to represent every output signal in a similar form. This means that any linear system can be completely described by how it changes the amplitude and phase of sinusoids passing through it. This information is called the system's frequency response (Smith, 1999).

In **Fig. 1.2,** an impulse, x[n], and the impulse response, y[n], which is output of a linear system, h[n], are shown both in the time domain and frequency domain. The illustration shows that FT's of x[n], h[n], y[n] can be taken and they can be represented in the frequency domain, as well as in the time domain. As it is seen, they are denoted X[f], H[f], Y[f] in the spectra, respectively. Also in **Fig. 1.2**, the inverse discrete FT is shown to transform the signals in spectra back to time domain. Since IDFT is not in the scope of this study, it will not be mentioned in detail.

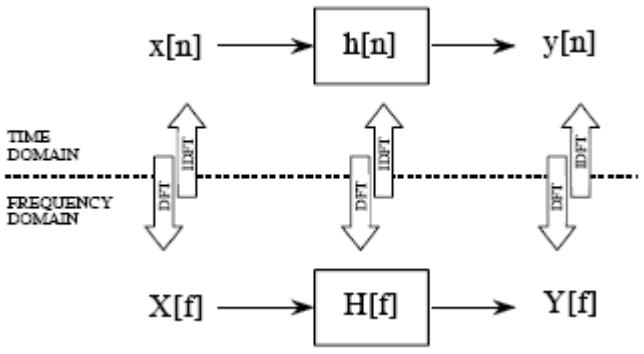

Figure 1.2—Comparing operations in time and frequency domains (Smith, 1999).

The frequency response term is used to describe the steady-state response to a sinusoidal input by a linear, time invariant system with zero initial conditions. The frequency response at one frequency is computed

as the ratio of the amplitudes of the FT of the output signal to the FT of the input signal at the specified frequency (Harman, 2000).

After the FT of the input is taken, the frequency response analysis is performed. These analyses are very popular since the sinusoidal inputs are very common in engineering applications. As noted earlier, any periodic signal of interest can be represented as a linear combination of sinusoidal components. Therefore, either stochastic or deterministic kind of flow rate data can be used throughout the applications in this study.

In the frequency domain, the input spectrum is multiplied by the frequency response, resulting in the output spectrum. That corresponds to a convolution in the time domain.

$$X(f) \times H(f) = Y(f) . \quad \text{.....(1.13)}$$

Where

X(f) = FT of the input (injection rate or voltage at the sending end)

Y(f) = FT of the output (production rate or voltage at the receiving end)

H (f) = Transfer function of the reservoir (frequency response)

Referring to **Fig. 1.2**, the mathematical expression of the transfer function, *H(f)*, which is the frequency response of a linear system, is noted already in Eq 1.7 in the previous sections:

$$H(f) = \frac{Y(f)}{X(f)} . \quad \text{.....(1.7)}$$

The transfer function is the frequency response of the output to a sinusoidal input in a linear system, *i.e* electrical circuit and reservoir. If the injection rate or voltage at the input end is an *impulse*, the production rate or voltage at the receiving end is called the *impulse response*. The discrete Fourier transform (DFT) of the impulse response is the frequency response.

We perform the evaluation of the transfer functions and the comparisons between analytical solutions (RCTF) and simulated reservoir applications (RTF) in the frequency domain.

Low-Pass filters

The *low-pass filters* are the sorts of frequency responses that are dealt here in spectral analyses through transfer functions. They are filters that allow low frequency components to pass whereas they block the high frequencies after a certain cut-off frequency. The full blockage of the high frequencies at a definite cut-off frequency is actually an ideal case. In most of the cases presented in this study, the stopband does not exist because it appears only in very compressible reservoir models, whereas mainly slightly compressible reservoir models are targeted in the applications. Usually filters consist of only stopband and transition band. The representation of the frequency response of a low-pass filter is available through calculation of the transfer function. Thus, there are two types of low-pass filters featured throughout the study, which belong to RC networks and reservoir models.

In evaluation of these filters, there are three important characteristics to describe filter performance as shown in **Fig. 1.3**. These are:

- Passband: It refers to the frequencies that pass through the filter. There should be no ripples in the passband in order not to let frequency amplitudes through the filter be changed.
- Transition band: It is a region between passband and stopband. To separate closely spaced frequencies, there has to be a fast roll-off, which requires the transition band be narrow.
- Stopband: It contains the frequencies that are blocked by the filter. To adequately block the stopband frequencies, there should be good stopband attenuation and be very close to zero with no ripples.

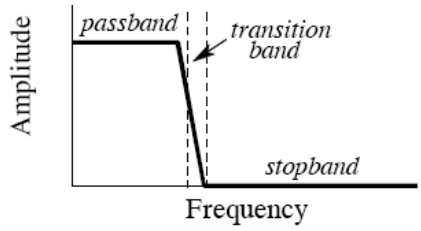

Figure 1.3—A low-pass filter representation, which shows passband, transition band and stopband (Smith, 1999).

The low-pass filters are important to identify the frequency response of an impulse by a linear system, which can be either RC network or reservoir throughout the study. As we will demonstrate by the transfer functions of these systems in Chapter II and III, these systems are also low-pass filters. In both of these systems, high frequency components are attenuated because of the compressibility and the capacitance terms that keep the low frequency components at the same magnitude. Since both RC networks and reservoir models are due to the same sort of attenuation in high frequencies, these systems can be compared with each other in a common frequency domain with regards to the changes in their energy levels.

1.5 Conclusions

1. Interwell connectivity studies indicate that conventional cross correlation techniques may not always provide the most accurate results due to the nature of the input data. Therefore, frequency domain applications, neural networks and multivariate regression analyses are performed in the literature. The major problems that remain unsolved in those studies are in the saturated reservoir cases, when the amount of injected fluid exceeds the amount of produced fluid, and when the bottom-hole pressures are fluctuating. In our study, we intend to investigate if multi-phase production, that occurs when bottom-hole pressure at the producer drops below the bubble-point pressure, affects the analogy that we apply by using RC analog devices in identification of fluid flow in simulated reservoir models.

2. The most important conclusion that we draw from sinusoidal flow rate applications is that the more recognizable a stimulus applied upon the reservoir is, the easier and more accurate reservoir identification is possible. Especially, when we deal with low-pass filters in the frequency domain, it is very crucial to keep the main signal with as little noise as possible. Therefore, we use sinusoidal flow rates, which are very commonly applied in electrical engineering practice to identify a linear system, to keep it simple to interpret the main signal during analyses in the frequency domain.

3. In this study, we apply an analogy between RC networks and reservoir systems owing to the fact that energy accumulation in both systems can be expressed similarly as stated in Eqs 1.1 through 1.4. The mutual relationship between those systems can be summarized as the following:
   - Storage of energy in these systems is due to the compressibility (reservoir) and the capacitance (RC network) terms.
   - High frequency components are attenuated due to the storage in the systems (low-pass filters).
   - There is the similarity of the governing equations which enables us to construct the analogy in dimensional RC models based on their coefficients.

4. On the basis of that analogy, we solve the transmission line equation analytically for 1D, and 2D RC models and use the storage equation for 0D RC model to compare them later on with the sinusoidal flow rate data obtained from reservoir simulations. The goal is to determine which network model behaves most similarly to the reservoir flow, and to investigate whether multi-phase production in the reservoir will affect the similarity.

CHAPTER II

ELECTRICAL ANALOGS TO SMALL COMPRESSIBILITY SITUATIONS

2.1 Introduction

As stated by Bruce (1943), an electrical device, which consists of a resistance and capacitance, can be used to simulate the fluid flow in a porous media. The capacitance placed in a circuit is capable of storing electrical energy in its field; likewise, reservoir rock and fluids act as a sponge that stores mechanical energy. **Table 2.1** is used to classify the correspondences between an electrical circuit and a reservoir rock and fluid system. This is a table summarizing the entire concept in terms of the terminology from both disciplines.

Table 2.1— Analogy of parameters between an electrical circuit and a reservoir is presented along with heat flow correspondences that help to understand 1D and 2D analytical solutions.

	Fluid Flow in Porous Media	**Electrical Flow in a Circuit**	**Heat Flow**
Governing Equation	$\frac{\partial^2 p}{\partial z^2} = \frac{\phi\mu c_t}{k}\frac{\partial p}{\partial t}$	$\frac{\partial^2 v}{\partial z^2} = RC\frac{\partial v}{\partial t}$	$\frac{\partial^2 T}{\partial z^2} = \frac{1}{\kappa}\frac{\partial T}{\partial t}$
Material Balance (Bruce, 1943)	$q_{net} = V_p c_t \frac{dp}{dt}$	$i_{net} = C_E \frac{dv}{dt}$	
Flux		$F(z,t) = -\frac{1}{RC}\left(\frac{dv}{dz}\right)$	$F(z,t) = -\kappa\rho c\left(\frac{dT}{dz}\right)$
Parameters	Flow Rate, q	Current, i	
	Pressure, p	Voltage, v	Temperature, T
	Transmissibility, $\frac{\mu\phi}{k}$	Resistance, R	
	Storage, $V_p c_t$	Capacitance, C	

This chapter is allocated for three different RC model analytical solutions, which we use ultimately in the identification of reservoir behavior. First of all, we present the derivation of the transmission line equation. Then, the analytical solutions to the transmission line equation are shown. We would like to note that we take advantage of the similarity of the mathematics of fluid, electrical and heat flow while solving the transmission line equation and forming the transfer functions. Therefore, throughout the study notice that both temperature (T) and voltage (V) represent the pressure (P) term.

2.2 Derivation of the Transmission Line Equation of a Resistance - Capacitance Network Model

The transmission line provides a medium allowing the current flow through a pathway between two terminals due to a difference in potentials. The following 1D, semi-infinite RC network (**Fig. 2.1**) is used for the derivation of the transmission line equation, which will be derived in terms of both current, *i* and voltage, *v*. The transmission line is assumed to have no inductance and no leakage. Resistance is in ohms; capacitance is in farads.

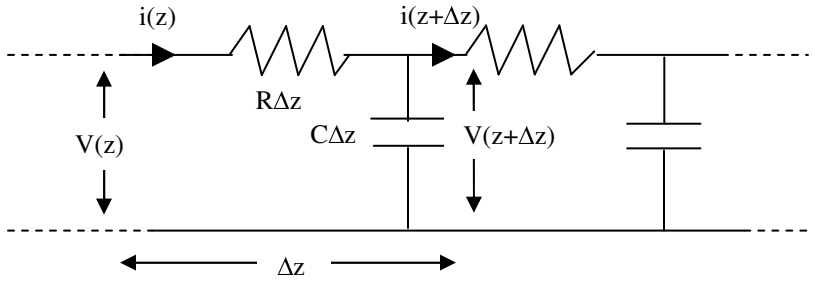

Figure 2.1—1D semi-infinite RC network setup for transmission line derivation.

Considering a distance of Δz between two points on a semi-infinite transmission line, the change in voltage (Eq. 2.2) and current (Eq. 2.4) are expressed respectively by Ohm's law (Eq. 2.1) and Kirchoff's law. Kirchoff's current law states that the algebraic sum of the currents entering any node is zero. And, Kirchoff's voltage law states that the algebraic sum of the voltages around any loop is zero.

$$v = iR\,. \quad (2.1)$$

For voltage:

$$v\left(z+\Delta z\right) - v\left(z\right) = -\left(R\Delta z\right) i\left(z\right). \quad (2.2)$$

Dividing both sides by Δz and taking the limit as $\Delta z \to \infty$, space derivative of voltage can be written:

$$\frac{\partial v}{\partial z} = -Ri\left(z\right). \quad (2.3)$$

For current:

$$i\left(z+\Delta z\right) - i\left(z\right) = -\left(C\Delta z\right)\frac{\partial v}{\partial t}. \quad (2.4)$$

Dividing both sides by Δz and taking the limit as $\Delta z \to 0$, space derivative of current can also be written:

$$\frac{\partial i}{\partial z} = -C\frac{\partial v}{\partial t}. \quad (2.5)$$

As it is noticed, the space derivatives of voltage and current depend on one another in Eqs 2.3 and 2.5. Both of them depend on only one independent variable, which is space, z. Therefore, the transmission line equation can be expressed in two ways.

First way is to differentiate Eq. 2.3:

$$\frac{\partial^2 v}{\partial z^2} = -R\frac{\partial i\left(z\right)}{\partial z}. \quad (2.6)$$

Substituting Eq. 2.5 into 2.6, the transmission line equation in terms of voltage takes the following form:

$$\frac{\partial^2 v}{\partial z^2} = RC\frac{\partial v}{\partial t}. \quad (2.7)$$

Second way to derive the transmission line equation in terms of current is to differentiate Eq. 2.5:

$$\frac{\partial^2 i}{\partial z^2} = -C\frac{\partial}{\partial z}\left(\frac{\partial v}{\partial t}\right). \quad (2.8)$$

Interchanging the order of differentiation on the right hand side results in:

$$\frac{\partial^2 i}{\partial z^2} = -C\frac{\partial}{\partial t}\left(\frac{\partial v}{\partial z}\right). \quad (2.9)$$

Substituting Eq. 2.3 into Eq. 2.9 gives the new form of the transmission line equation:

$$\frac{\partial^2 i}{\partial z^2} = RC\frac{\partial i}{\partial t}. \quad (2.10)$$

The transmission line equation is a second-order partial differential equation. Since the coefficient of the time derivative on the right hand side is assumed constant and not a function of either voltage or current, it is a linear PDE, just like the diffusivity equation (**Table2.1**).

We want to clarify that the similarity between the diffusivity equation and the transmission line equation is not the reason of the analogy between RC networks and reservoirs. It is mainly because of the storage of the energy in the systems, as explained earlier. The similarity between the governing equations enables us only to construct a link between RC networks and reservoirs through the coefficients of the time derivatives. Additionally, we mention correspondences to the heat flow equation here in Chapter II because we use the analytical solutions of 1D and 2D RC models from the heat equation solutions of Carslaw and Jaeger, 1986.

2.3 RC Network Analytical Solutions

Three types of solutions of the governing transmission line equation (Eq. 2.7) are represented in this section. These solutions are respectively for 0D (lumped) RC model, 1D RC model, and 2D RC model. In each subsection, the ultimate goal is to show the RCTF.

2.3.1 Zero Dimensional Solution

This solution is based on a tank model where a material balance is applied on the RC network model in accordance with Kirchoff's Laws. The change in voltage is expressed in terms of only the time derivative. Reservoir engineering applications of this type of RC model are reported by Bruce (1943), Wahl *et al.* (1962), and Al-Yousef *et al.* (2005). The RC model of interest is sketched in **Fig. 2.2**. The correspondence between electrical flow and fluid flow is already shown on **Table 2.1** in terms of the storage term due to the relationship between the capacitance and the compressibility.

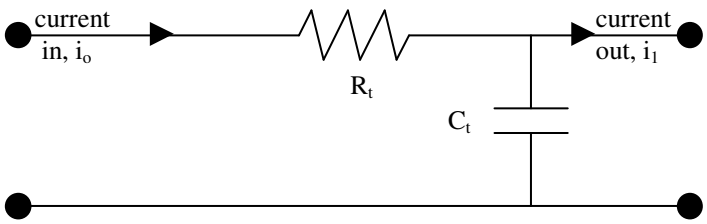

Figure 2.2—A lumped electrical model with elements for total resistance (R_t) and total capacitance (C_t).

Assuming sinusoidal excitation of angular frequency ω, the transfer function of a series circuit can be explained by an impedance divider. Impedance means the ratio of voltage to current (from Ohm's Law). Simply, RC network is divided into two parts by a voltage. And, the voltage differences at both ends of the circuit are expressed in terms of impedances. The voltage at the sending end (V_{in}) represents the

impedance of both resistor and capacitor as shown in Eq 2.11, whereas the voltage at the receiving end (V_{out}) consists of only the capacitor's impedance (Eq. 2.12).

$$V_{in}(f) = \frac{1}{j\omega C} + R \; . \quad \text{.....(2.11)}$$

$$V_{out}(f) = \frac{1}{j\omega C} \; . \quad \text{.....(2.12)}$$

Where

ω = Angular frequency, radian/sec

j = Imaginary unit

Recalling the frequency response of a linear system to an input, which is given in Eq. 1.7, the transfer function of a lumped RC network can be given by the following equation:

$$H_{0D}(f) = \frac{V_{out}(f)}{V_{in}(f)} \; . \quad \text{.....(2.13)}$$

Where

$V_{out}(f)$ = Voltage at the receiving end, volts

$V_{in}(f)$ = Voltage at the sending end, volts

$H_{0D}(f)$ = Transfer function of a lumped RC network

Substituting the impedances of the resistor and the capacitor, the new form of the transfer function is given below (Irwin, 2002):

$$H_{0D}(f) = \frac{1}{1 + j\omega RC} \; . \quad \text{.....(2.14)}$$

This analytical solution, besides 1D and 2D applications, has a different approach, assuming the model of interest a dimensionless tank model. The important point is that this model, which is being lumped into zero dimensions, can be representative of an originally multi-dimensional model.

2.3.2 One Dimensional Solution

The solution is based on a linear semi-infinite 1D RC network (**Fig. 2.3**), where voltage is preferred to be harmonic function of time. Using a periodic function at the inner boundary condition makes it a better solution since FT's are used to decompose the flow rates, which are specifically selected to be sinusoidal functions of time. The corresponding reservoir flow rate generations are explained in Chapter III.

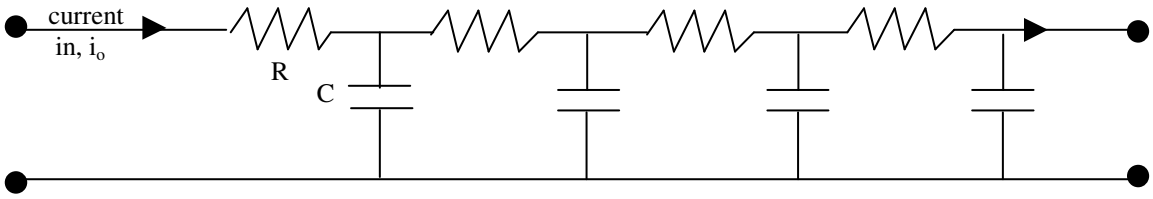

Figure 2.3—A 1D electrical model with elements for resistance (R) and capacitance (C).

The 1D solution to the second-order PDE (Table 2.1) is given in the following form (Carslaw and Jaeger, 1986, p.65):

$$v\left(z,t\right) = Ae^{j\omega t}\left[e^{-z\sqrt{\omega RC/2}}e^{-zj\sqrt{\omega RC/2}}\right]. \quad \text{.....(2.15)}$$

This is the voltage distribution across 1D semi-infinite RC network. Since we use flow rate data from the simulated reservoir models in the frequency domain analysis, we should compute the flux of the current flowing across a unit cross sectional area. The flux of current at a unit cross sectional area in 1D electrical flow is given in the following form (**Table 2.1**):

$$F\left(z,t\right) = -\frac{1}{RC}\left(\frac{dv}{dz}\right). \quad \text{.....(2.16)}$$

Thus, we obtain the voltage gradient from the space derivative of voltage distribution in Eq. 2.15:

$$\frac{dv}{dz} = -A(1+j)\sqrt{\frac{\omega RC}{2}}e^{-z(1+j)\sqrt{\frac{\omega RC}{2}}}e^{j\omega t} . \quad (2.17)$$

Hence, we can express the current flux in an electrical flow in the following way:

$$F(z,t) = -\frac{A}{RC}(1+j)\sqrt{\frac{\omega RC}{2}}e^{-z(1+j)\sqrt{\frac{\omega RC}{2}}}e^{j\omega t} . \quad (2.18)$$

The transfer function of a linear system is available through the ratio of the output to the input:

$$H_{1D}(z) = \frac{F(z,t)}{F(0,t)} . \quad (2.19)$$

Where

$H_{1D}(z)$ = Transfer function of the 1D RC network

$F(z,t)$ = Flux at the receiving end of the RC network (output)

$F(0,t)$ = Flux at the sending of the RC network (input)

The current flux at the sending end of the 1D RC network is given as:

$$F(0,t) = -\frac{A}{RC}(1+j)\sqrt{\frac{\omega RC}{2}}e^{j\omega t} . \quad (2.20)$$

Ultimately, the transfer function of the 1D linear RC network takes the form of Eq. 2.22:

$$H_{1D}(z) = e^{-z(1+j)\sqrt{\frac{\omega RC}{2}}} . \quad (2.21)$$

$$H_{1D}(z) = e^{-z\sqrt{\frac{\omega RC}{2}}}e^{-zj\sqrt{\frac{\omega RC}{2}}} . \quad (2.22)$$

The first term on the right hand side is the magnitude of a complex number. It represents the attenuation of the voltage. The second term is the complex part of the number, which represents the phase change. In this study, only the attenuation part of transfer functions is going to be used.

2.3.3 Two Dimensional Solution

The analytical solution is based on a radial 2D RC network and relatively more complicated than the previous models (**Fig. 2.4**) but it supplies a better alternative to identify more complex systems. The radial solution of the transmission line equation requires a unit line source solution with the following periodic source assumption:

$$v\left(r=0,t\right)=\rho c e^{i\omega t}\ . \quad \text{.....(2.23)}$$

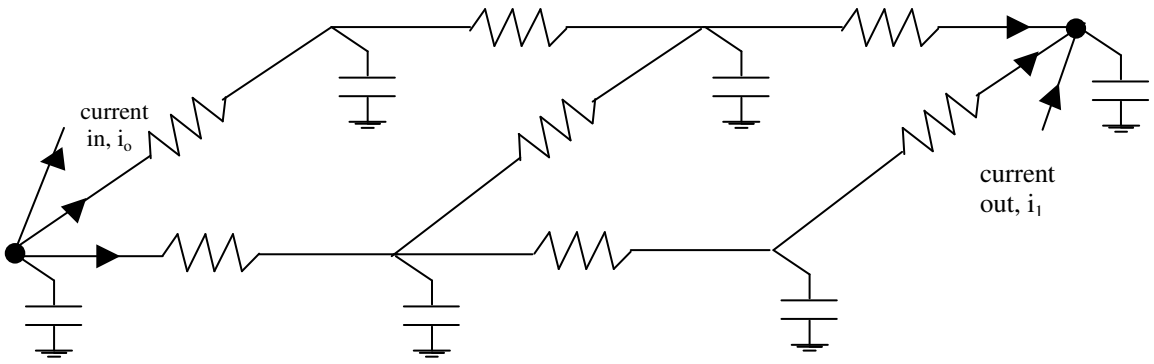

Figure 2.4—A 2D electrical model with elements for resistance (R) and capacitance (C).

The 2D solution to the second-order PDE (**Table 2.1**) is given in the following form (Carslaw and Jaeger, 1986, p.263):

$$v\left(r,t\right)=\frac{RC}{2\pi}e^{j\omega t}\mathrm{K}_O\left[\sqrt{j\omega RC}r\right]. \quad \text{.....(2.24)}$$

Where

$K_0(r)$ = Modified Bessel function of the second kind, zero order

The flux of current over a cylinder in 2D electrical flow is given in the following form:

$$F\left(r,t\right)=-\frac{1}{RC}\left(\frac{\partial v}{\partial r}\right)2\pi r\ . \quad \text{.....(2.25)}$$

The voltage gradient:

$$\frac{dv}{dr}=\frac{RC}{2\pi}\sqrt{j\omega RC}e^{j\omega t}\mathrm{K}_1\left[\sqrt{j\omega RC}r\right]. \quad \text{.....(2.26)}$$

Where

$\mathrm{K}_1(r)$ = Modified Bessel function of the second kind, first order

Thus, the flux at the receiving end of the network:

$$F\left(r,t\right)=-r\sqrt{j\omega RC}e^{j\omega t}\mathrm{K}_1\left[\sqrt{j\omega RC}r\right]. \quad \text{.....(2.27)}$$

The flux at the sending end of the network:

$$F\left(0,t\right)=-e^{j\omega t}\ . \quad \text{.....(2.28)}$$

Hence, the transfer function of the 2D RC network model is given as the ratio of fluxes at the receiving and sending ends of the network:

$$H_{2D}(r)=\frac{F\left(r,t\right)}{F\left(0,t\right)}=r\sqrt{j\omega RC}\mathrm{K}_1\left[\sqrt{j\omega RC}r\right]. \quad \text{.....(2.29)}$$

2.4 RC Transfer Functions

We exhibit the applications on RC models in this section to demonstrate how we present the analytical solutions of RC models in this study. Through the calculation of a transfer function, we can perceive ideas on how effective a circuit performs because of a voltage potential.

Recalling the fact that RC network is a low-pass filter, we interpret the RCTF'ss according to the characteristics of low-pass filters, which are mentioned in Chapter I. Using Eqs. 2.14, 2.22, and 2.29, 0D, 1D, and 2D transfer functions show different behavior (**Figs. 2.5a, 2.5b,** and **2.5c**). In general, all figures present a smooth passband until the start of the transition region. This means the low frequency components are able to pass through the circuit with no change in their amplitudes until a certain cut-off frequency when attenuation of high frequency components, is reached. In most of the cases we deal, a flat stopband does not exist, which means there is not complete blockage of high frequencies, but only attenuation.

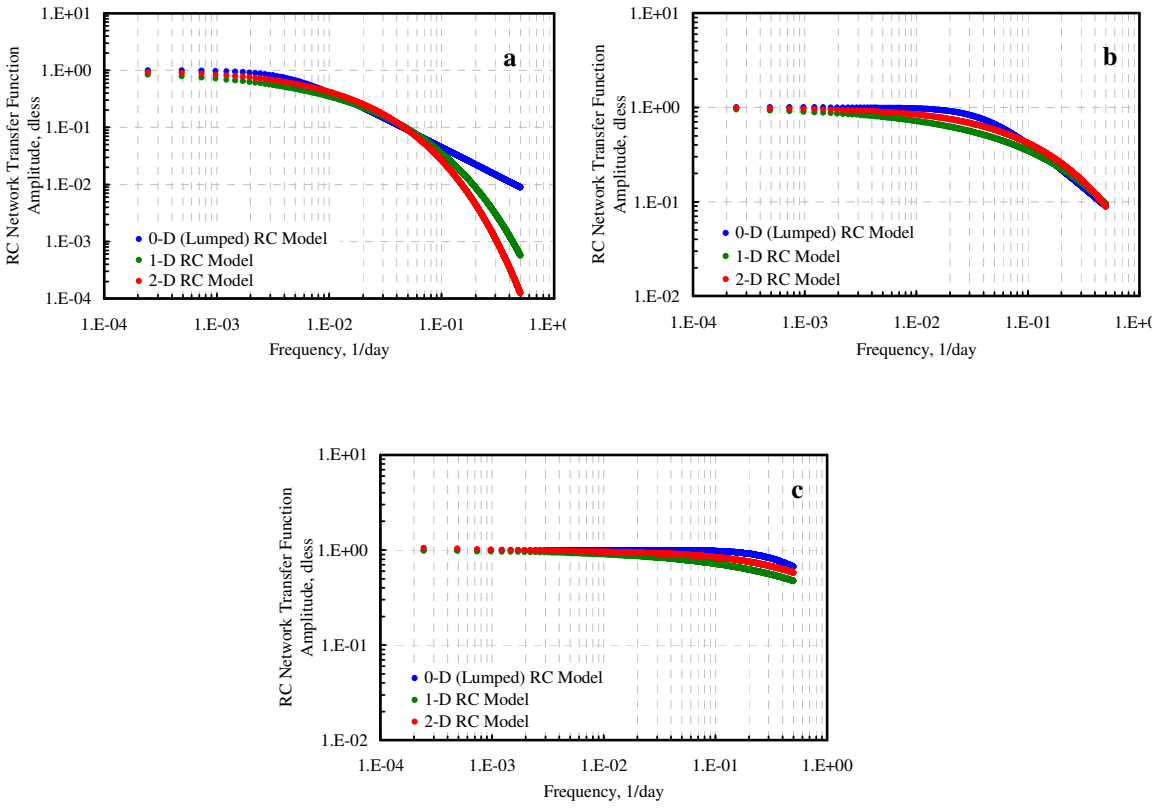

Figure 2.5—Three RC model representations in transfer functions when the distance is 460m for 1D and 2D models for (a) RC=14.5 sec/m^2 (b) RC=1.45 sec/m^2 (c) RC=0.145 sec/m^2. Change in the low-pass filter characteristics can be seen as we decrease the RC coefficient an order of magnitude on each figure.

The analytical solutions that we produced for 1D and 2D RC models are functions of the *RC* coefficient and the distance between two measurement points whereas, for 0D model, there is only the *RC* coefficient that needs to be specified. In **Figs. 2.5a** through **2.5c**, we demonstrate RCTF'ss for three *RC* coefficients. These coefficients are an order of magnitude different from each other to show how attenuations of the functions lessen drastically and the stopbands become longer as we decrease the *RC* coefficient. The range of the frequencies is determined to be 0 to 0.5 1/day considering that the maximum frequency produced by the DFT is 0.5 1/day.

Fig. 2.5a is the representative of a case where capacitance is very high, which means the circuit is capable of storing a lot of energy. As the characteristics of a low-pass filter are considered, the stopband is smooth, the transition region is broad and the attenuation is large, especially for the 2D model. All three models have very low cut-off frequencies meaning only very small range of frequencies are kept in the same magnitude through passband. Most of the frequencies, which begin from ~0.002 1/day are attenuated in these RC circuits. The main difference between 0D, 1D, and 2D models is the degree of attenuation. In 0D model, the attenuation is only 2 orders of magnitude, whereas it goes up to 4 orders of magnitude in 2D model. This means there is more filtering performed in 1D and 2D models over the range of frequencies considered.

Fig. 2.5b represents the case where the capacitance is reduced an order of magnitude, which yields an *RC* coefficient of 1.45 sec/m^2. As a result of reducing the coefficient, the circuit lessens dramatically its ability to attenuate the high frequencies. This can be deduced from a higher cut-off frequency ~0.02 1/day (for 0D model) and less attenuation in high frequency components, which is only an order of magnitude. The difference between the three models is very small: the 1D and 2D model behavior is the same and the 0D model is the most distinguishable result with a more specific cut-off frequency where the start of the attenuation is easily discerned. In all, in comparison with the higher *RC* coefficient application, the attenuation reduced very much.

Fig. 2.5c is the application of the smallest *RC* coefficient on three RC models. The capacitance has the least influence on the circuit among all representations. It has almost no storage capability. Therefore, the attenuation is almost none when compared with the highest *RC* coefficient application in **Fig. 2.5a**. The cut-off frequency increased from 0.002 1/day (highest *RC* case) to 0.2 1/day (lowest *RC* case) for 0D model. The characteristics of the models have changed enormously because the attenuation has lost its effect on the signals due to a lower *RC* coefficient. The changes in the attenuation and the passband have become relatively very small.

2.5 Conclusions

1. At high *RC* coefficient in **Fig. 2.5a**, all analytical solutions have almost same passbands; the distinguishing parameter is the degree of attenuation.

2. At middle *RC* coefficient in **Fig. 2.5b**, proximity among analytical solutions increases and they all present the same amount of attenuation. The only parameter that can help us to characterize models is the cut-off frequency, where the transition region begins in a low-pass filter.

3. At small RC coefficient in **Fig. 2.5c**, the changes in the attenuation are relatively smaller and the lengths of the passbands are longer; however, we can distinguish characteristics of the low-pass filters with different cut-off frequencies and attenuations easily.

4. Considering that we will use those analytical solutions to identify fluid flow for the reservoir models that we simulate for sinusoidal flow rates, we expect 1D RCTF to be similar with the fluid flow in a narrow conduit and 2D RCTF to be similar with the multi-dimensional fluid flow in a large drainage area. 0D RCTF has the capability of matching with all reservoir models that 1D and 2D are supposed to match because it is a lumped model that can describe pressure distribution with regards to the time derivative of the voltage and pressure that is free of dimension.

CHAPTER III

DETERMINATION OF RESERVOIR TRANSFER FUNCTIONS

3.1 Introduction

A reservoir transfer function's (RTF) role in this study is to see which one of the three RC transfer functions (RCTF) can be used to determine interwell connectivity. Previously, we describe that RCTF are calculated for reservoir systems with small compressibility values. Here, we simply explain what methods we applied to come up with our choice of RTF and what we did to avoid spurious results in the frequency spectra to be able to make accurate comparisons between RTF and RCTF.

In this chapter, we applied deterministic, stochastic and random flow rate data to come up with the best possible RTF with the least margin of error that causes ambiguous results in the determination of the interwell connectivity.

3.2 Spectral Analyses on Reservoir Flow Rate Data

The reservoir model, on which this interwell connectivity study is based, consists of one injector and one producer well in a homogeneous reservoir. As we explain in Chapter I, we infer the connectivity information from the relationship of the coefficients of RTF and RCTF. Therefore, it is very important to make correct predictions from their relationship in the frequency spectra.

We analyze the spectra in terms of the change in their amplitudes of high and low frequency components. And, we calculate RTF (Recall Eq. 1.7) to analyze the amount of attenuation of high frequency components in low-pass filters.

3.3 Choices of Injection Rates Used in Spectral Analyses

In each of the following applications, we used a reservoir geometry of 1500ft x 150ft x 20ft (**Fig.3.1**) to simulate the production rates in accordance with the particular injection flow rate. And, we used the

reservoir simulation results only from the single-phase (only water) production in a homogenous and isotropic reservoir to develop the understanding needed to explain RTF. The reservoir parameters that we used for the reservoir simulation is stated in **Table 3.1**.

Table 3.1—Reservoir parameters used in the numerical simulation for all types of rate profiles.

Reservoir dimensions	1500x150x20	ft^3
Grid refinement	150x50x5	
Gridblock dimensions	10x3x4	ft^3
Interwell distance	1508	ft
Production phase	water	phase
ϕ	0.1	d.less
k	100	md
μ_w	1	cp
B_w	1.01	RB/STB
C_w	1.00E-05	1/psi
BHP @producer	250	psi
Initial pressure	1470	psi
Duration	4096	days

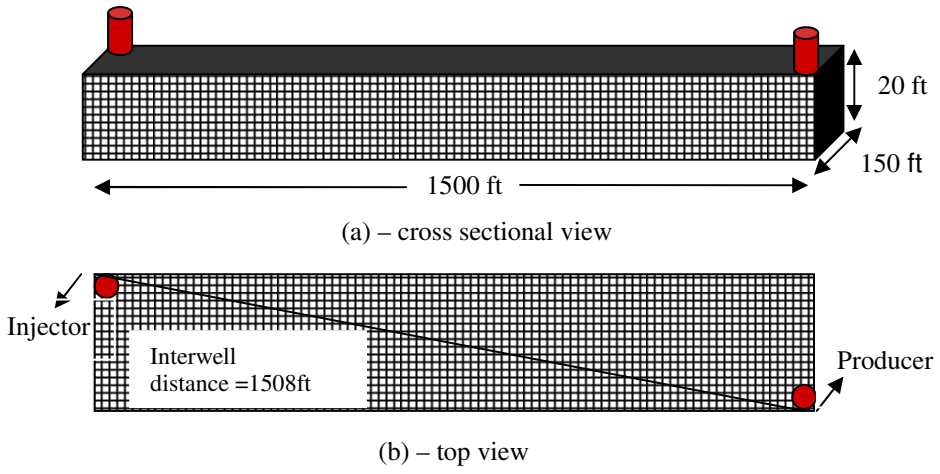

Figure 3.1—Reservoir model used in the numerical simulations.

3.3.1 Sinusoidal (Deterministic) Flow Rates

Our main initiative in using FT's is its ability to decompose an arbitrary function into its sinusoids. Hence, using Fourier method, one can obtain very successful and precise results in the frequency spectrum by using a deterministic function and transforming this function into the frequency domain by Fourier method. (Recall **Fig. 1.1**) Therefore, we used pure sinusoidal flow rates to investigate the effect of reservoir behavior as a low-pass filter on the frequency components.

In order to understand the phenomenon in the frequency domain better, we simplified the injection rate profile by using pure sinusoidal components with no noise. We used four perfectly sinusoidal functions with single frequency and a fifth function that is the sum of the four sinusoids to understand how the amplitudes of those particular frequencies change after simulating the fluid flow in a reservoir (**Table 3.1**). Frequency components that we used in this analysis are shown in **Table 3.2**. The flow rates generated for this part of the study are presented in **Fig. 3.2**.

The Fourier spectra of those four distinct injection flow rates are in **Fig. 3.3**. The only crucial information that one should perceive from this figure is only the magnitudes of the following specified frequencies, 0.04, 0.05, 0.1 and 0.2 1/day stated in **Table 3.2**.

Table 3.2—Frequency components used to generate 5 different injection rate profiles.

Injection Rate No.	Frequency, 1/day
1	0.04
2	0.05
3	0.10
4	0.20
5	0.04, 0.05, 0.1, 0.2

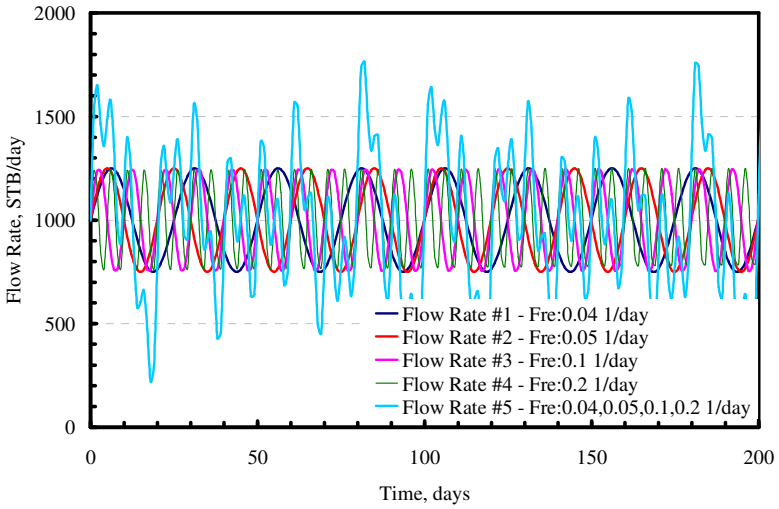

Figure 3.2—Pure sinusoidal injection rates generated in the time domain.

The magnitudes of the particular frequencies are at the correct frequency and at the same amplitude, 512,000. Therefore, the slope of the four amplitude values is 0. The fifth flow rate is a double check to see if we calculated the magnitudes correctly in Matlab and also to check if the response goes under any change when data includes more than one frequency component. This is the spectrum of the injection flow rates.

The Fourier spectra of the production rates changes drastically (**Fig. 3.4**). The amplitudes of those four frequencies are attenuated. This figure shows that the amplitudes decreased due to the low-pass filtering process in the reservoir, which is actually the effect of the compressibility factor. The low level of noise in the injection rates has increased by three orders of magnitude due to the noise added by the simulation. RTF is shown in **Fig. 3.5**.

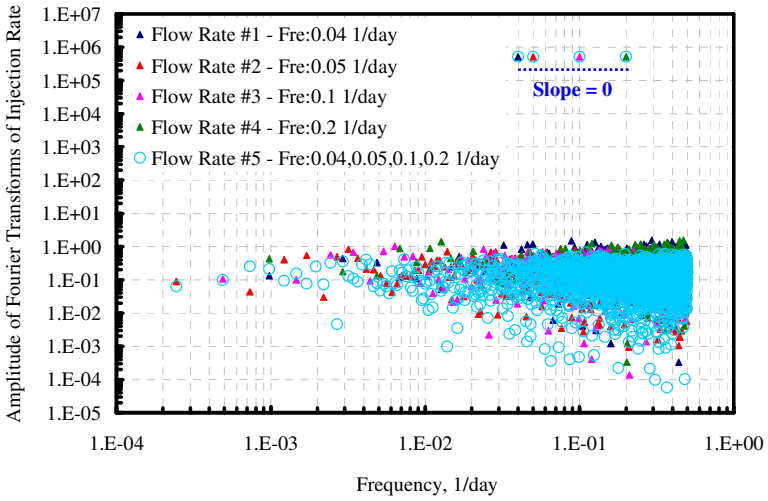

Figure 3.3—Sinusoidal injection rates in the frequency domain.

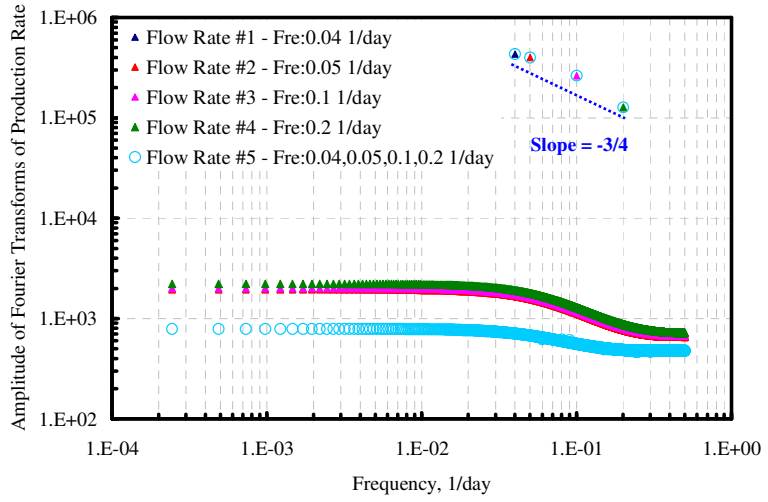

Figure 3.4—Simulated sinusoidal production rates in the frequency domain.

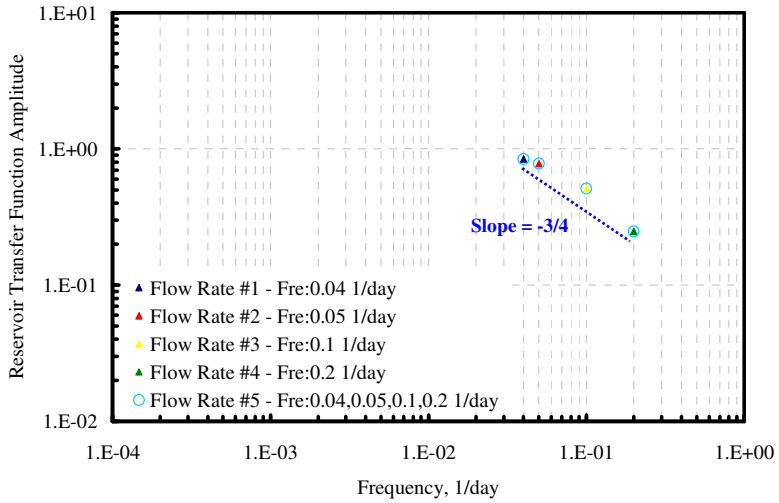

Figure 3.5—RTF produced from sinusoidal flow rates after removing the noise.

This example shows that:

- Because we can easily discern the frequency contents of the main signal, the use of deterministic input functions such as sinusoidal functions gives very accurate results in the frequency domain.
- The application of sinusoidal functions avoids the noise in spectrum making the main signal easily detectable.
- An injection signal with more sinusoidal components is desirable to better define RTF.

3.3.2 Periodic (Stochastic) Flow Rates

We generated the periodic flow rate randomly; however we specified some constraints on initial injection rate, amplitude, cycle. We also added noise and phase to the data. As a result of this procedure, we used a stochastic flow rate (**Fig.3.6**), which is randomly generated due to the constraints tabulated in **Table 3.3** for the analysis of RTF. We used the numerical simulation parameters stated in **Table 3.1** to produce the water production rates in **Fig. 3.6**.

Table 3.3—Constraints used in random periodic flow rate generation (Albertoni, 2002).

Min. Initial Rate (bbl/d)	500
Max. Initial Rate (bbl/d)	1500
Initial Rate (bbl/d)	793.5922
Phase (rad)	2.254553
Min. Amplitude (bbl/d)	30
Max. Amplitude (bbl/d)	100
Amplitude (bbl/d)	54.07199
Min. Cycle (mths)	7
Max. Cycle (mths)	30
Cycle (mths)	8.812222
Noise	70

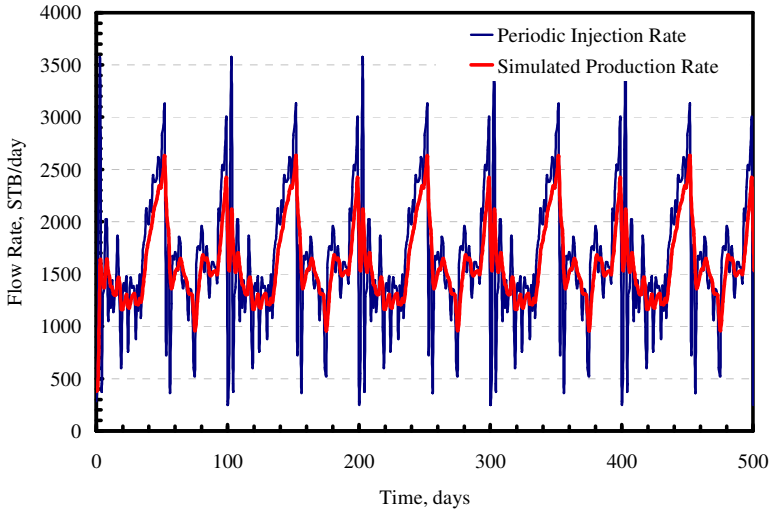

Figure 3.6—Generated periodic injection rate and the simulated water production rates in the time domain.

The periodic flow rate, which we used in the analyses, consists of various frequencies; the biggest cycle, which is distinguishable in the time domain, repeats every 100 days and it corresponds to the lowest frequency component (0.01 1/day) in the spectrum (**Fig. 3.7**). Despite the fact that not every cyclicity can be seen in the time domain (**Fig. 3.6**), the frequency domain representations in **Figs. 3.7a** and **3.7b** make it easier to distinguish all the cyclicities in the data. The semi-log plot emphasizes the changes of the high frequency amplitudes more than the log-log plot. By this way, the most dominant frequencies in the data, which are 0.01 and 0.02 1/day, are easily discerned. In the log-log plot, it is harder to see the changes in

higher frequencies; therefore semi-log plot is also presented. These figures exhibit what happens to frequencies during fluid flow in the specified reservoir when inverse diffusivity coefficient (IDC) is set to 1.45 sec/m^2. Reservoir being a low-pass filter attenuates the high frequency components and the Fourier spectra of the production and injection rates exhibit the fluid flow in terms of frequencies.

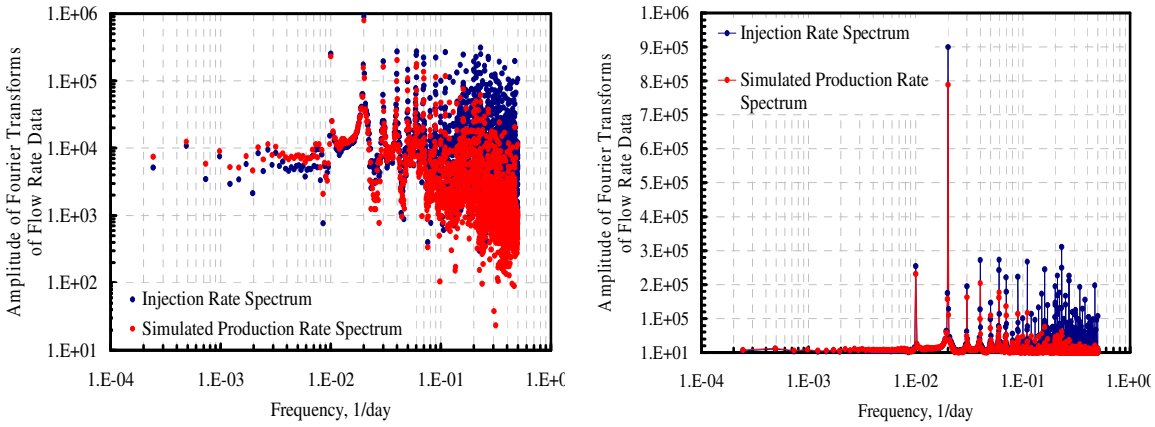

Figure 3.7—Periodic injection rate and the simulated production rate spectra after FT's are computed. (a) log-log plot (b) semi-log plot.

Dealing with this sort of data set, which has a lot of frequencies in it, requires a very good resolution in the frequency domain. To be able to maintain such good resolution to distinguish all the frequency components in a time series, it is very crucial to increase the number of data points, thereby decrease the space between each frequency component. Increasing the number of data points in this part of analysis would be useful to discern each one of the high frequency component. However, increasing the number of points in time series costs us higher run times during simulation, since computation at every day was performed at the numerical simulation.

RTF in **Fig. 3.8** summarizes the whole procedure ending up with a nice low-pass filter behavior, which means there is a smooth passband in low frequencies and a transition band, where attenuation of high

frequencies is performed. The attenuation at high frequencies is about 2 orders of magnitude. However, the cycles being very dominant in the data does not allow for a precise interpretation in RTF spectrum.

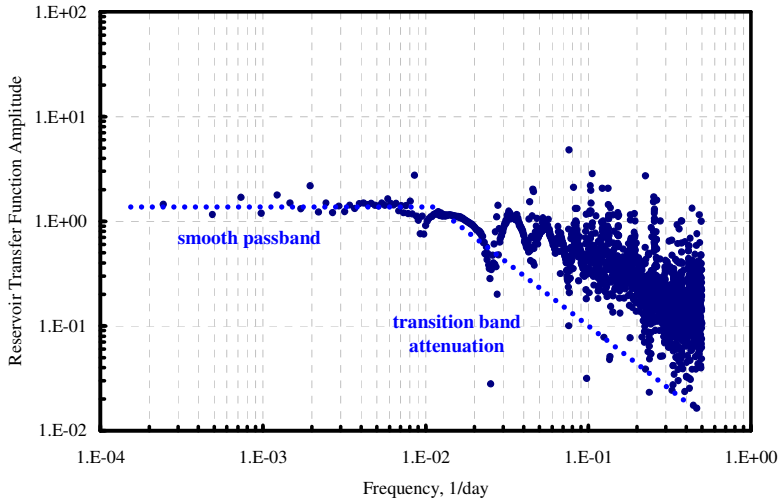

Figure 3.8—RTF produced from a periodic flow rate data.

RTF analyses on the periodic flow rate data does not result a satisfactory answer to form an analogy with the RC models; therefore, we extended the analyses towards the investigation of perfectly sinusoidal rate data.

RTF produced by stochastic periodic flow rates (**Fig. 3.8**) is not wrong, but does not supply a firm basis to construct an analogy between RC models. They can provide only qualitative information about a RTF. However, what we need to use is a quantitative approach to be able to compare an RCTF with that of a reservoir.

3.3.3 Random Flow Rates

We used a normally distributed random series (mean=1000 STB/day, standard deviation=200 STB/day). to investigate the impact of random data on RTF. We used this random series as an injection rate profile

to simulate the reservoir given the parameters in **Table 3.1** and to produce the simulated water production rates. The time domain injection and production rates are shown in **Fig. 3.9.**

Fig. 3.10 is the representation of the flow rates in the frequency domain, showing the attenuation of high frequency components of the production rates. The amplitudes of the low frequency components suffer almost no change, whereas there is about two orders of magnitude change in amplitudes of high frequency components. This is a typical response of a low-pass filter, as mentioned in Chapter I.

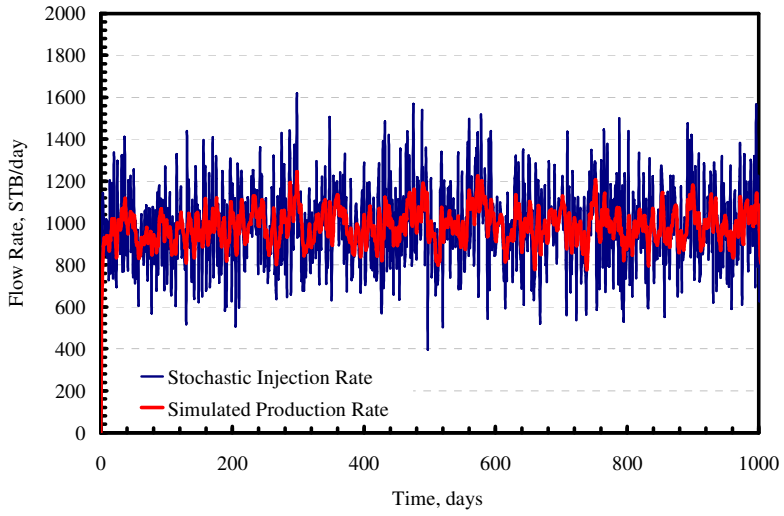

Figure 3.9—Randomly generated injection rate and the simulated water production rates in the time domain.

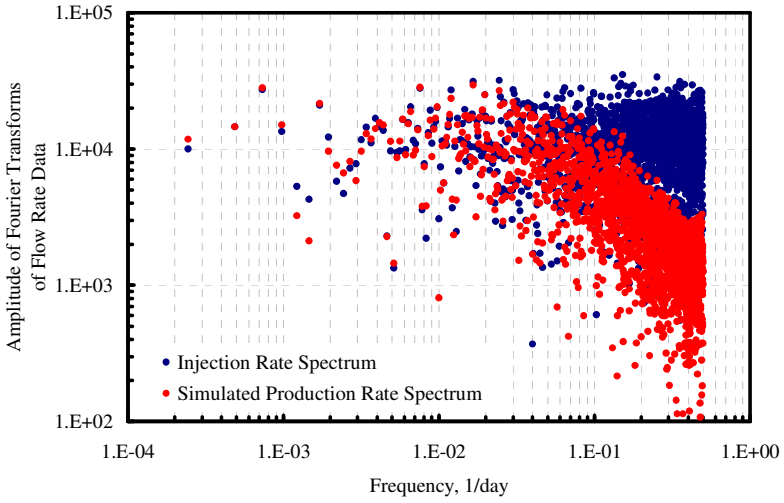

Figure 3.10— Random injection rate and the simulated production rate spectra after FT's are computed.

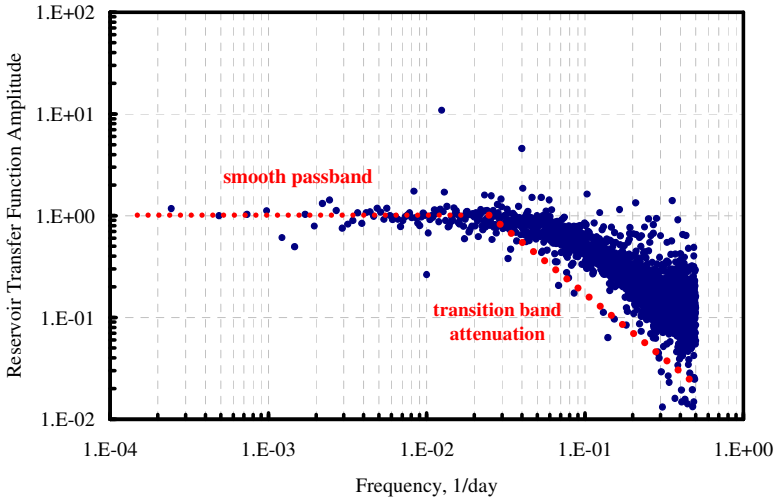

Figure 3.11—RTF produced from random flow rates.

RTF in **Fig. 3.11**, makes it easier to discern the degree of attenuation shown in **Fig. 3.10**. The amount of the attenuation is directly related to the diffusivity parameters that affect the flow pattern. Therefore, the compressibility, which is the parameter of interest due to its analogy to the capacitance term in RC

models, has a considerable effect on the amount of attenuation. IDC under the specified conditions in **Table 3.1** is 1.45 sec/m^2 and produces 2 orders of attenuation in high frequencies of the random rate spectrum.

The amount of noise in this case is large because:

- The data set itself is already a randomly generated noise.
- The discretization error is generated through the numerical simulation.
- Although it is very small and adjustable in the software by the number of digits of the decimal numbers, the round-off error caused by fast Fourier algorithm in Matlab are existent.

Resolution in the frequency domain

While using a pure random time series in our analysis, we did not aim to discern a main signal in the frequency domain. However, our initiative behind applying this time series is based on the fact that if the impulse response of the random time series is infinitely long, the data points in the frequency response should be infinitesimally close together, which results in a continuous line in the frequency domain (Smith, 1999). Theoretically, this implies that the FT of an infinitely long random time series forms a flat line in the frequency domain. This way it would be easier for us to plot any kind of change in RTF with regards to the flat injection rate spectrum. However, the discrete time series, which we use in the random data analysis, consists of only 4096 points. Thus, the injection rate spectrum in **Fig. 3.10** is not a flat line and it deviates from the theory by ending up with a lot of noise. Therefore, the simulated production rate spectrum also has a lot of noise with some additional noise coming from the numerical simulation and Matlab computations.

This is an issue related to the resolution of points in the frequency domain. In this study, considering the amount of time that a reservoir simulation takes to run and the main signal, which is the injection rate, should be a power of 2 as mentioned in any Matlab manuals, we selected 4096 data points to produce the data sets to be utilized in the analyses.

Convolution with the Blackman window function

To reduce the amount of noise, which is caused by the randomness of the time series in RTF spectrum, we used convolution with Blackman window. It is a basic moving average filtering method that aims to smooth the noise. We convolved the random injection rate **(Fig. 3.9)** profile with a 7 point Blackman window shown in **Fig.3.12**. Besides Hamming window, Blackman window is a very common window function used in digital signal processing to remove the noise from the main signal in the time domain. The Blackman window function is given in Eq. 3.1:

$$w(n) = 0.42 - 0.5Cos\left(\frac{2\pi n}{N-1}\right) + 0.08Cos\left(\frac{4\pi n}{N-1}\right) \quad \text{.....(3.1)}$$

Where

$w(n)$ = Blackman window function

N = Width of the window

n = Integer with values $0 \le n \le N-1$

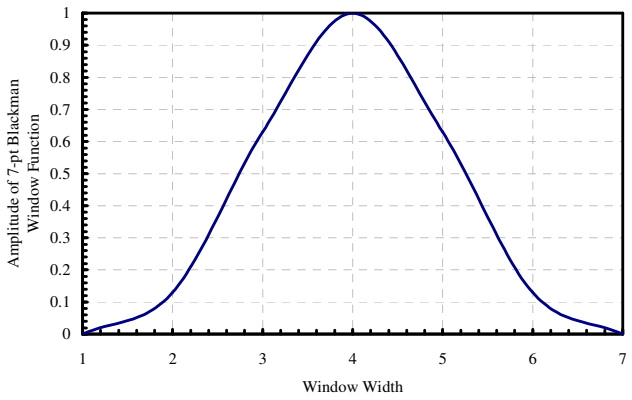

Figure 3.12— 7 point Blackman window function, which we used to convolve the injection rate spectrum in **Fig. 3.9**.

Fig. 3.13a shows the convolved injection rate and the corresponding simulated production rate spectra. **Fig. 3.13b** shows RTF in the case when the random injection rate profile (**Fig. 3.9**) is convolved by a 7-point Blackman window function (**Fig. 3.12**). Then, we used the convolved injection rate profile to

simulate the water production rates. Taking the FT's of the convolved injection rates and the simulated production rates; we calculated RTF and plotted as in **Fig. 3.13b**.

The only difference between **Fig. 3.11** and **3.13b** is using the raw injection rate profile in the former and the convolved rate profile in the latter. Despite the smoothing operation in the time domain, the difference between two figures is not as we expected. The convolution with the Blackman window function (Eq.3.1) does not cause a dramatic improvement in the spectrum by removing most of the noise in the frequency domain. The filtering process performs very well and attenuates the high frequency components in **Fig.3.13b**; however, the spread in the spectra that is caused by the randomness of the input does not improve. Eventually, the moving average filtering has not performed well in the frequency domain as much as it has in the time domain.

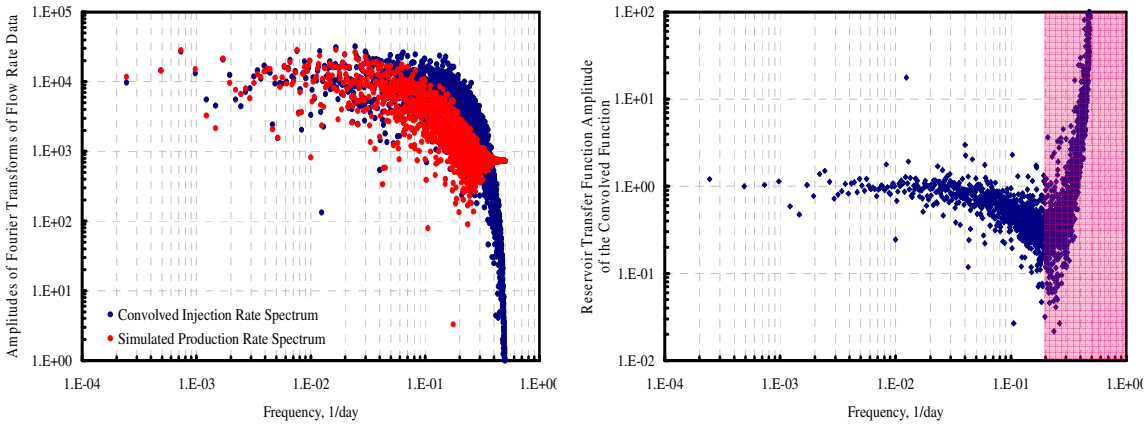

Figure 3.13— Convolved injection & simulated production rates spectra (a) and RTF produced from a convolved random flow rate data(b).

Especially, the frequencies higher than 0.2 1/day are assumed to be erroneous because a transfer function can not be bigger than 1. In a linear system, it is not possible to receive a steady-state impulse response amplitude higher than the impulse amplitude itself. The reason of this erroneous region in **Fig. 3.13b** is due to applying two filters simultaneously to a system. These two filters are respectively 7-point

Blackman function and the reservoir itself. The attenuation caused by a Blackman function is ~4 orders of magnitude as seen in convolved injection rate spectrum in **Fig. 3.13a**; whereas the attenuation caused by a reservoir simulation is only ~2 orders of magnitude as seen in simulated production spectrum in **Fig. 3.13a**. Thus, the difference of 2 orders of magnitudes between these two filters appears as an erroneous region in RTF.

As a result of using random injection rates in the analyses, the nature of the data does not allow us to do precise interpretation in RTF spectrum with respect to the RCTF. Therefore, deterministic rate profiles are investigated if better results can be obtained from RTF spectra to construct a link between RC models and reservoir.

3.4 Reservoir Transfer Functions

The development of this type of RTF is based on the study performed with pure sinusoidal functions in the previous section. Taking advantage of FT's' success to decompose a sinusoidal function into its sinusoids perfectly well, we made up of a function with 30 different sinusoids to produce an injection rate to be used throughout the remainder of this work. The frequencies that we used to generate this set of injection rate are shown in **Table 3.4**. According to the list of frequencies, the biggest frequency is 0.4899 cycle/day, which has 2.04 sample/cycle; on the other hand the smallest frequency is 0.00098 cycle/day, which has 1020.41 sample/cycle. The range of frequencies is important because it has to be broad enough so that RTF can be descriptive at both very low and very high frequencies.

Table 3.4—30 frequency components used in the injection rate profile.

No.	Frequency, 1/day	No.	Frequency, 1/day	No.	Frequency, 1/day
1	0.00098	11	0.04004	21	0.22217
2	0.00171	12	0.05005	22	0.24438
3	0.00244	13	0.06006	23	0.25000
4	0.00513	14	0.07007	24	0.26001
5	0.00732	15	0.08008	25	0.27002
6	0.01001	16	0.09009	26	0.28003
7	0.01514	17	0.10010	27	0.30029
8	0.02002	18	0.14014	28	0.35010
9	0.02515	19	0.17993	29	0.39990
10	0.03125	20	0.19995	30	0.48999

We generated a sinusoidal injection rate profile with an initial flow rate of 1000 stb/day and an amplitude of 30 stb/day. We display it in **Fig. 3.14** along with the simulated water production rates. We used the reservoir conditions given in **Table 3.1** to simulate the homogeneous single-phase production at the producer. The production rates are being smoothed by the filtering process in reservoir due to the compressibility effect, which is set to 1e-5 1/psi. As a result, the sharp edges of the injection flow rate are filtered and they no longer exist in the simulated production rates.

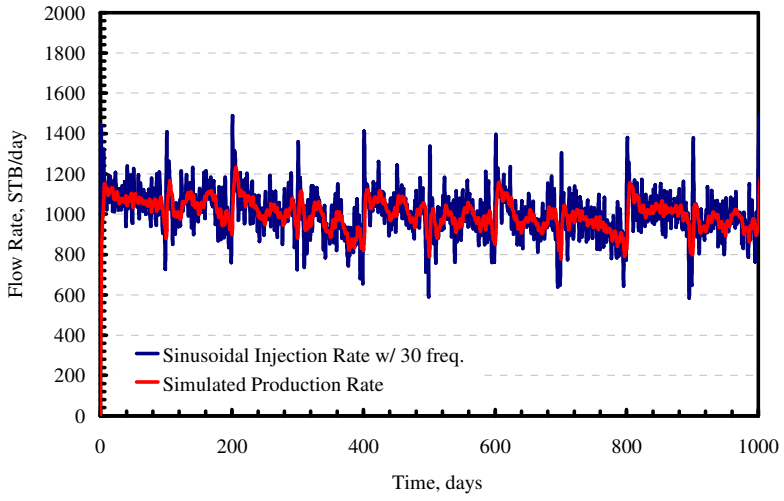

Figure 3.14— Sinusoidal injection rate generated with 30 frequency components and the correspondent simulated production rates.

We display the frequency-amplitude representation of the data sets (**Fig. 3.14**) in **Fig. 3.15.** The attenuation at the high frequency components is marked only about an order of magnitude, which is related to IDC set at 1.45 sec/m^2.

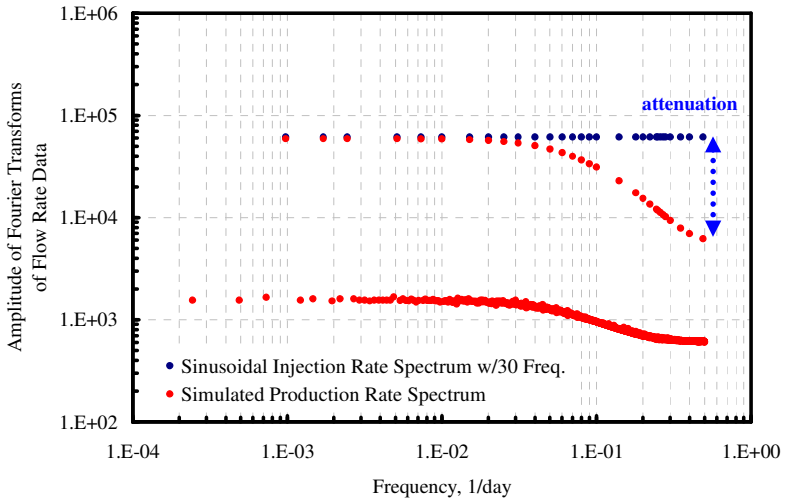

Figure 3.15— Sinusoidal injection rate spectrum generated with 30 frequency components and the correspondent simulated production rate spectrum.

RTF of the 30 frequency components is shown in **Fig. 3.16**. This representation clearly shows the low pass filtering effects of the reservoir.

We also performed an application of the same injection rate with some noise added over the data to check the availability of the same RTF. The amount of noise that we added to data set is ~10% of the total input. **Fig. 3.17a** displays the conventional RTF after noise is added over the sinusoidal injection rate. It is very hard to recognize the main signal in this spectrum. However, the main idea of using specific sinusoidal components in the input data reveals its advantage when we plot only these points in the frequency domain (**Fig. 3.17b**). It is very obvious that using only these points in the graph at the specified frequencies is very useful in identifying the main reservoir behavior during the displacement process, even though the process is very noisy.

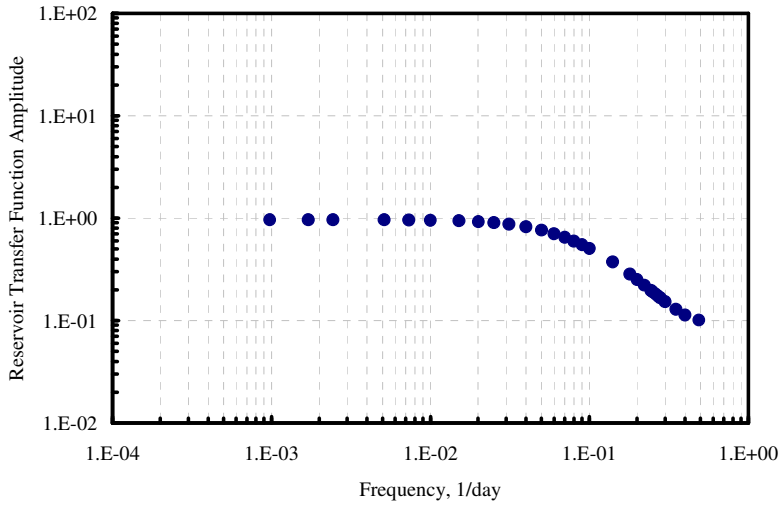

Figure 3.16—RTF produced from sinusoidal flow rate data based on 30 frequencies.

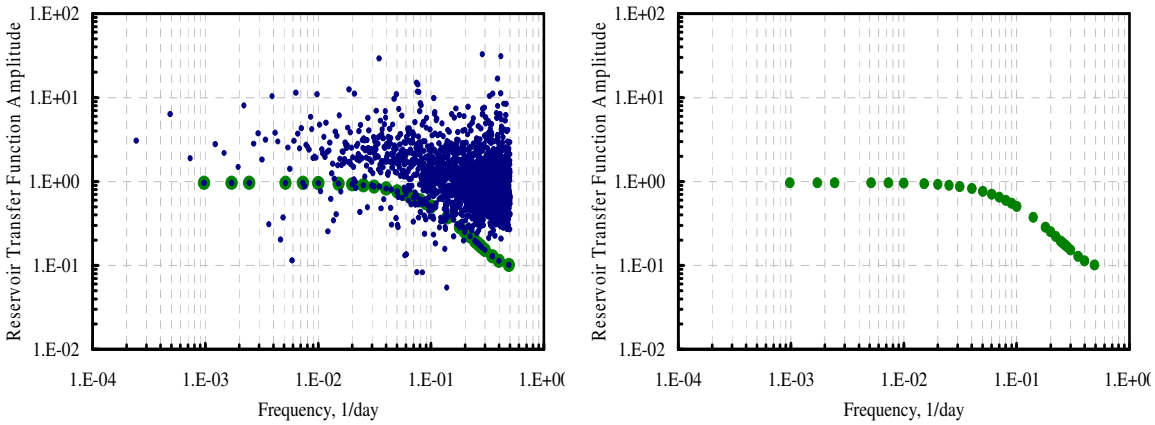

Figure 3.17—RTF produced from noisy sinusoidal flow rate data w/30 frequencies. (a) Noisy representation (b) 30 frequency representation.

3.5 Conclusions

Determining suitable injection signals for evaluation of RTF has been achieved.

1. Possible sources of noise throughout the applications cause wide ranges of spread at every frequency.

Overall, possible sources of noise in the study can be stated as the following:

- Data set is already incorporated with noise.
- The discretization error generated through the numerical simulation.
- The round-off errors caused by fast Fourier algorithm in Matlab.

2. Because noise masks the main signal by causing a wide range of spread in the spectrum, stochastic and random flow rates can be used for only qualitative purposes in the study. The spread of the noise is caused by the randomness of the data sets.

3. For quantitative purposes, sinusoidal flow rates are advantageous because of the use of FT's and the analogy we use against RC networks.

4. For the rest of the study, we have selected a sinusoidal injection rate with 30 specified frequencies as the injection rate to ensure that there is no noise masking the impulse response in the frequency domain.

5. The number of frequency components that we specified at the input function should be arranged by trial and error to find the optimum number that represents passband, cut-off frequency, transition region and stopband. For this study, 30 frequencies are enough to represent the functions.

CHAPTER IV

VALIDATION OF THE PROPOSED METHOD FOR CONNECTIVITY ESTIMATION

4.1 Introduction

We calculated RCTFs (RCTF) based on three analytical models to compare the spectral performance of several displacement processes with these analytical solutions. The ultimate goal is to select the analytical solution which best represents the reservoir behavior and predict the interwell connectivity.

Another objective is to determine which displacement cases emulate the spectral behavior of any of the three RC networks and to evaluate their effects on estimating interwell connectivity if there are deviations from the assumed conditions.

4.2 Reservoir Models Used in Simulation Analysis

We used a standard reservoir geometry, as we used in Chapter III, in the applications unless otherwise stated (**Fig. 3.1**). This is a 5 layer model allowing fluid flow in y-direction and limited flow in z-direction. The injector is located in gridblock at (1, 1); the producer is located at (150, 50). The interwell distance is about 1508 ft (~460m). The gravity effect is on. Waterflooding is performed in each simulation. 1% random error is added to the injection rate which is based on 30 frequencies. Simulated production rates given the reservoir parameters, which will be specified in each section, are modeled in Eclipse by E100.

We used a fine discretisation to reduce the truncation error and the instability as much as possible. The fully implicit simulation option is used in Eclipse Black Oil Simulator (E100) to produce the simulated values. The fully implicit option takes longer than the IMPES option, due to three unknowns per gridblock, but performs better when big fluctuations exist in the rate profile. The validation of the simulation model is detailed below.

We investigated three displacement processes: water displacing water, water displacing oil, and water displacing oil and gas. And, we used applications from different reservoir geometries, such as narrow and

large reservoirs. Finally, we represented RTF from each application and compared them with RCTF and discussed the implications for connectivity estimations.

4.2.1 Simulation Model Validation

Model validation is necessary to ensure stable and accurate answers from the numerical reservoir simulations.

The criterion to test whether the results are stable is to compare the production rates of the producer from two following distinct runs:

- The case when the injector is turned off. There is only primary depletion. (Q_{in_off})
- The case when the injector is turned on. The producer is supported by the injector.(Q_{in_on})

The production rates, when the injector is on, should be higher than the case when the injector is off. Initial tests showed that this was not the case for the early times of a reservoir simulation. Therefore, very small gridblock and timestep refinements were used to overcome this problem. **Table 4.1** shows the grid refinements, timesteps and the mobility ratios, used throughout the sensitivity analyses. The reservoir parameters used in the simulation model are shown in **Table 4.2**.

Table 4.1—Reservoir parameters tested throughout the sensitivity analyses.

Grid Refinement	15x10x1	
	15x10x2	
	15x10x2	
	150x10x5	
	150x10x10	
	150x30x5	
	150x50x5	
Timestep refinement	1	Day
	0.1	Day
	0.01	Day
Mobility Ratio	1	d.less
	10	(μ_o=10cp)

Table 4.2—Reservoir parameters used in the simulation model validation.

Reservoir dimensions	1500x150x20	ft^3
Interwell distance	1508	ft
Production phase	water, dead oil	
ϕ	0.1	d.less
k_x, k_y	100	md
k_z	1	md
μ_w	1	cp
B_w	1.01	RB/STB
C_w	1.00E-04	1/psi
	1.00E-05	1/psi
	1.00E-06	1/psi
μ_o	1	cp
B_o	1.07	RB/STB
C_o	1.00E-04	1/psi
	1.00E-05	1/psi
	1.00E-06	1/psi
C_f	1.00E-08	1/psi
BHP @producer	250	psi
Initial pressure	1470	psi
Constant injection rate	160	STB/day
S_{or}	0.2	d.less
S_{wc}	0.35	d.less

The sensitivity analyses, using 0.1 day of timestep and 1e-5 1/psi total compressibility, show (**Fig. 4.1**) that the problem does not occur at favorable mobility ratio at all. At unfavorable mobility ratio (**Fig. 4.2**); however, the problem appears at the very early life of the reservoir up to 2 days. The problem increases despite finer timesteps when we use larger compressibility fluids. (**Fig. 4.3**)

Making both timestep and gridblock improves the results, but it requires very long run times. Therefore, we used the 150x50x5 grid and 0.1 day timestep in the displacement process simulations.

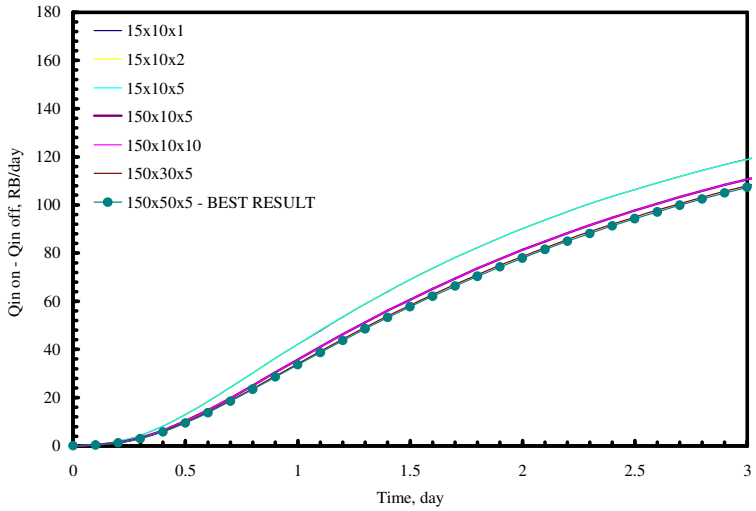

Figure 4.1—Flow rate difference in the cases when tstep=0.1day, mobility ratio=1, C_t=1e-5 1/psi for different reservoir grid dimensions.

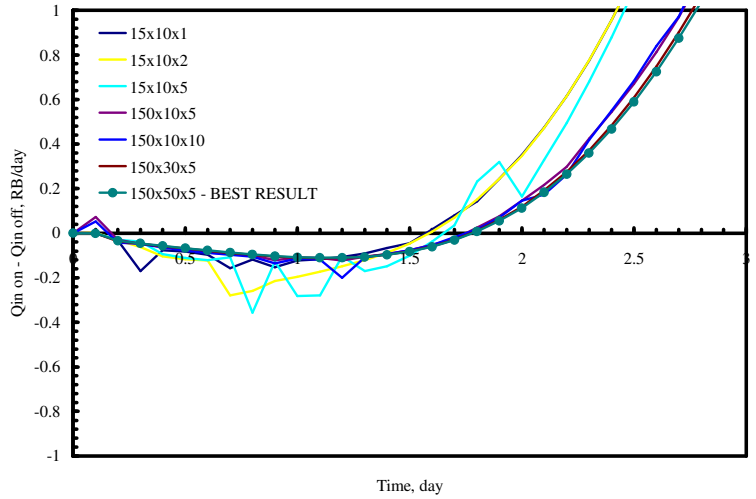

Figure 4.2—Flow rate difference in the cases when tstep=0.1 day, mobility ratio=10, C_t=1e-5 1/psi for different reservoir grid dimensions.

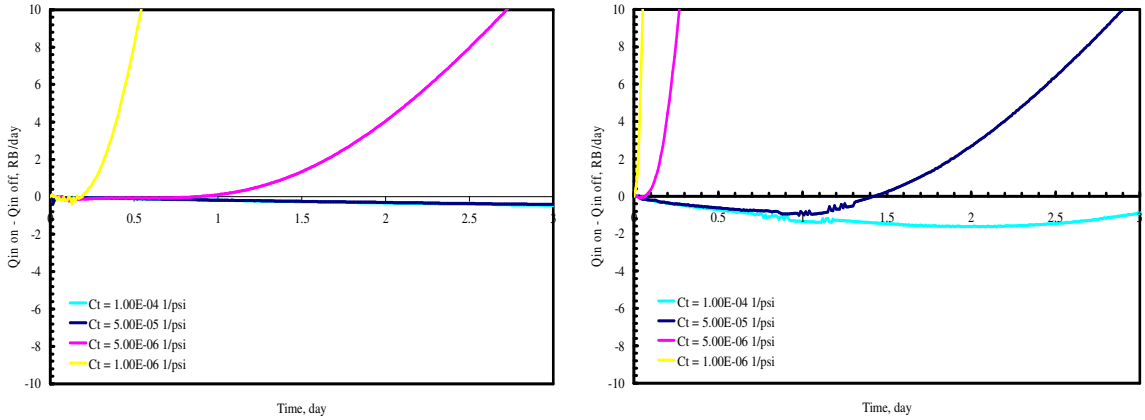

Figure 4.3— Flow rate difference between two cases when (a) unfavorable mobility ratio=10 tstep=0.01day; (b) favorable mobility ratio=1 tstep=0.01 day.

4.3 Single-phase (Water-only) Production Case

A water-only case forms a basis for comparison with the more realistic cases considered later. It involves the least amount of heterogeneity and represents a situation where the assumptions of the analytical solutions are met. Even though the reservoir is kept as a homogeneous model throughout the entire work, producing one more phase and including the relative permeability curves into the model creates heterogeneity in the system.

According to the reservoir parameters (**Table 4.3**), the inverse diffusivity coefficient (IDC) varies between 1.45e-1 sec/m^2 and 7.25e+0 sec/m^2. The lower the compressibility (**Fig. 4.4**), the higher is the transfer function amplitude. This implies the filtering ability of the reservoir lessens as the compressibility effect gets smaller. In the most compressible system, the high frequency values have ripples in the stopband due to the discretisation error generated by the numerical simulation.

Table 4.3—Reservoir parameters used for single-phase reservoir simulation.

Production phase	water	
ϕ	0.1	d.less
k_x, k_y	100	md
k_z	1	md
μ_w	1	cp
B_w	1.01	RB/STB
C_w	5.00E-05	1/psi
	1.00E-05	1/psi
	5.00E-06	1/psi
	1.00E-06	1/psi
BHP @producer	250	psi
Initial pressure	1470	psi
Duration	4096	days

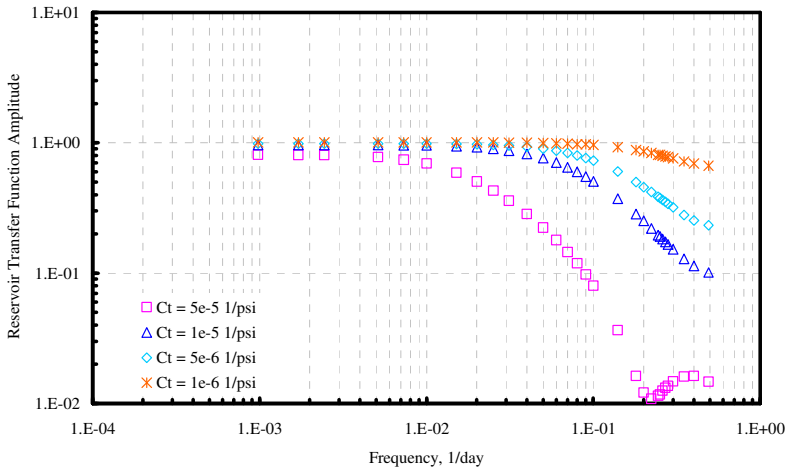

Figure 4.4—RTFs for single-phase production under various total compressibility values.

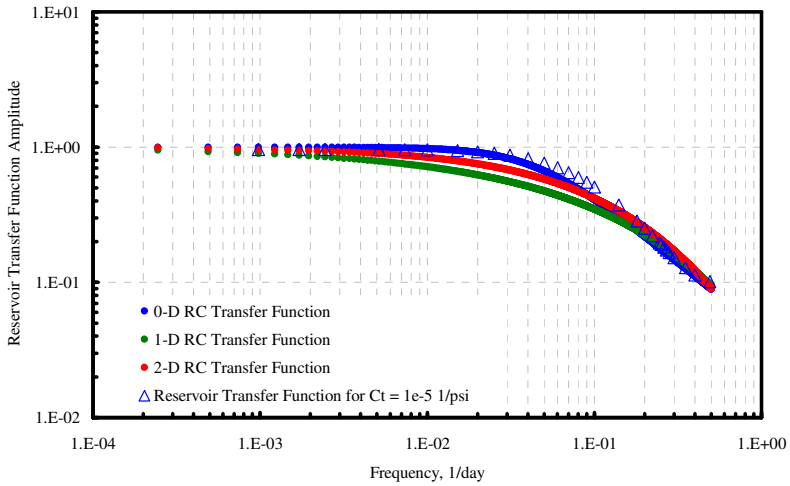

Figure 4.5—Comparison between three RCTFs (*RC*=1.45e+0 sec/m^2) and RTF for C_t=1e-5 1/psi when IDC=1.45e+0 sec/m^2.

The three analytical models and the RTF (**Fig. 4.5**) indicate that the 0D lumped model represents the reservoir behavior better than the other two solutions. In this case, the 2D and 1D model solutions underestimate RTF, whereas 0D solution fits the frequency cut-off and the transition region in high frequencies very well.

In other cases (**Fig. 4.6**), the 0D lumped model provides the best approximation to the transfer functions of slightly compressible homogeneous systems.

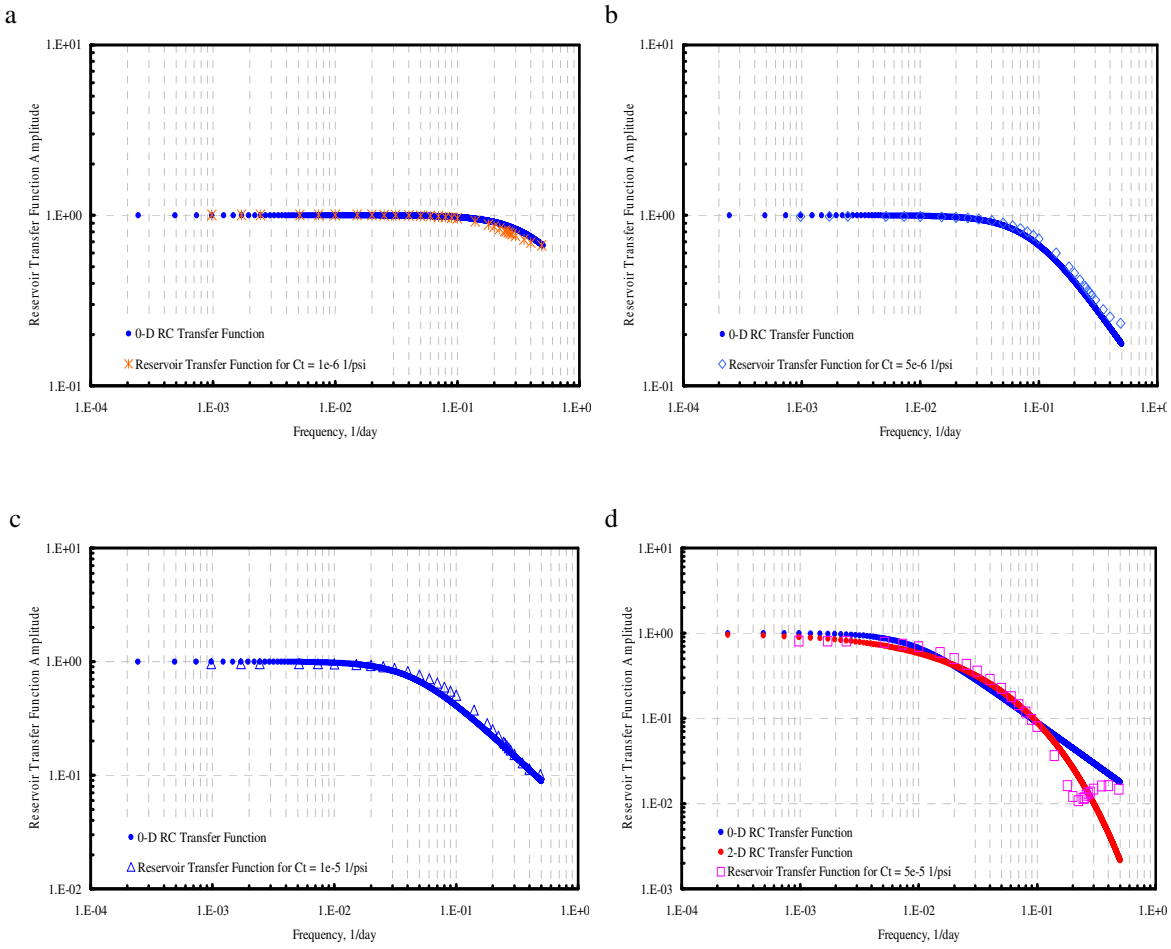

Figure 4.6—Comparison between RCTF and RTF for (a) C_t=1e-6 1/psi (b) C_t=5e-6 1/psi (c) C_t=1e-5 1/psi (d) C_t=5e-5 1/psi.

When the total compressibility is between 1e-5 1/psi and 1e-6 1/psi (**Figs 4.6a-6c**), the lumped RC solution matches RTF very well. However, when the system gets more compressible (**Fig. 4.6d**), the lumped model loses its ability to match the reservoir behavior and 2D model fits the fluid flow behavior better. In the most compressible system, the 2D model is more descriptive for the frequency cut-off and the transition region of the RTF.

As IDC increases, the attenuation in frequency spectrum increases because the reservoir rock has more potential to accumulate reservoir fluids in its media. In this example, we keep the porosity, permeability and viscosity value same and, modify only the total compressibility factor. Therefore, the change in the

attenuation as a result of the accumulation is caused by the compressibility factor. We can conclude from these analyses that 2D analytical solution is better than the other solutions to describe the reservoir behavior when high IDC values are used in the applications.

The analogy between these two media ensures that *RC* coefficient should be equal to the estimated IDC to infer the connectivity in terms or ϕ/k as seen in **Table 4.4**. If RCTF does not match RTF, then we adjust the *RC* coefficient of the analytical model to approximate the reservoir behavior. In such a case, we assign the modified *RC* coefficient to the estimated IDC, which yields the estimated ϕ/k values from the analogy between RC networks and reservoir.

For single-phase systems, we matched all RTFs with an analytical solution with no modification on the coefficients because the assumptions of the simple reservoir met the assumptions of the analytical solutions. We present the inferred values of diffusivity parameters in terms of ϕ/k in **Table 4.4**.

Table 4.4— The IDC in each case is compared with the *RC* coefficient that is used to calculate the analytical solution. Since the analytical solutions match with RTFs very well, no modification is done to the IDC. Therefore, the IDC, the *RC* coefficient and the estimated IDC values are equal to each other. Given the C_t and μ values, ϕ and k relationship is calculated from the IDC equation.

C_t 1/psi **Fig. 4.4**	IDC sec/m^2	RC sec/m^2	RC Model **Fig. 4.6**	Estimated IDC sec/m^2	$Ct.\mu$ cp/psi **Table 4.2**	Estimated ϕ/k 1/md
1.00E-06	1.45E-01	1.45E-01	0D	1.45E-01	1.00E-06	1.00E-03
5.00E-06	7.25E-01	7.25E-01	0D	7.25E-01	5.00E-06	1.00E-03
1.00E-05	1.45E+00	1.45E+00	0D	1.45E+00	1.00E-05	1.00E-03
5.00E-05	7.25E+00	7.25E+00	2D	7.25E+00	5.00E-05	1.00E-03

4.4 Two-phase Production Cases

We simulated the following two-phase fluid systems to evaluate their spectral behavior:

- Dead oil and water production
- Dry gas and water production

4.4.1 Dead Oil and Water Production Case

We reduced the injection rates by a factor of 10 from those of the base case. We show the relative permeability curves and the reservoir parameters that are applied in the models in **Fig. 4.7** and **Table 4.5**, respectively.

We used total fluids production rates for the transfer function calculations (**Fig. 4.8**). In this application, we modeled slightly compressible systems with total compressibility values of 5.5e-6, 2.8e-6 and 5.5e-7 1/psi. The IDC given the reservoir parameters varies between 7.98e-1 sec/m^2 and 7.98e-2 sec/m^2.

The most compressible system with total compressibility of 5.5e-6 1/psi shows similar high-frequency behavior to that seen in the high diffusivity water-only case.

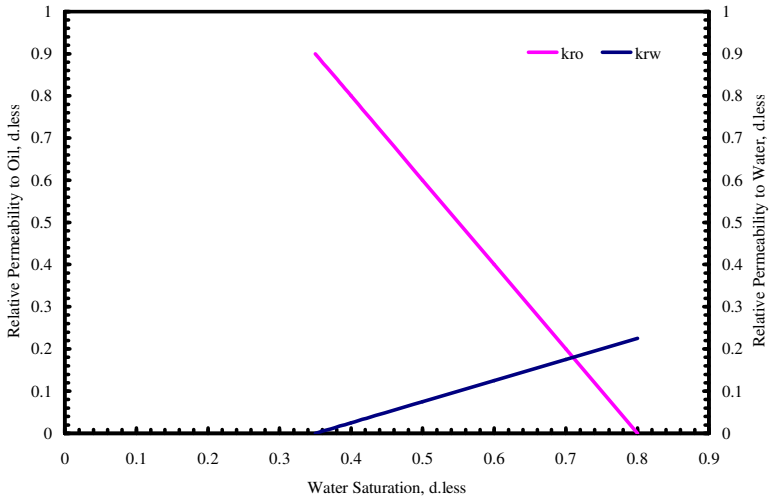

Figure 4.7—Relative permeability curves that we used in dead oil and water production.

Table 4.5—Reservoir parameters that we used for dead oil and water production.

Production phase	water, dead oil	
ϕ	0.1	d.less
k_x, k_y	100	md
k_z	1	md
μ_w	1	cp
B_w	1.01	RB/STB
C_w	1.00E-05	1/psi
	5.00E-06	1/psi
	1.00E-06	1/psi
μ_o	1	cp
B_o	1.07	RB/STB
C_o	1.00E-05	1/psi
	5.00E-06	1/psi
	1.00E-06	1/psi
C_f	1.00E-08	1/psi
S_{or}	0.2	d.less
S_{wc}	0.35	d.less
BHP @producer	250	psi
Initial pressure	1470	psi
Duration	4096	days

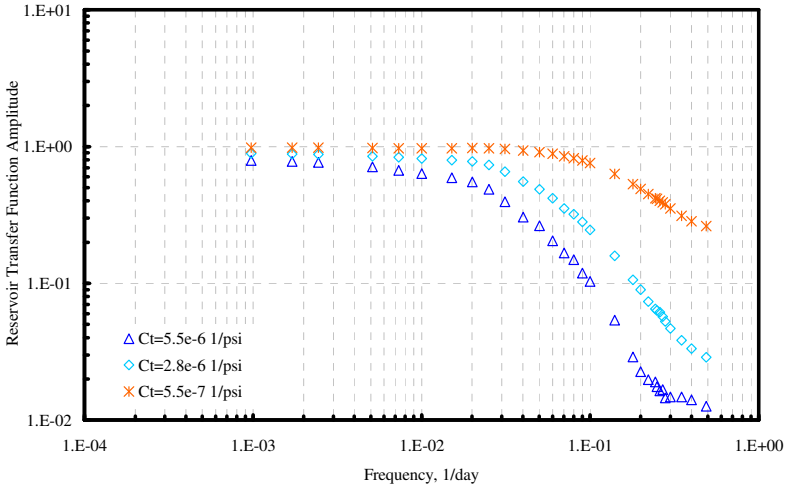

Figure 4.8— Transfer functions for dead oil and water production under various total compressibility values.

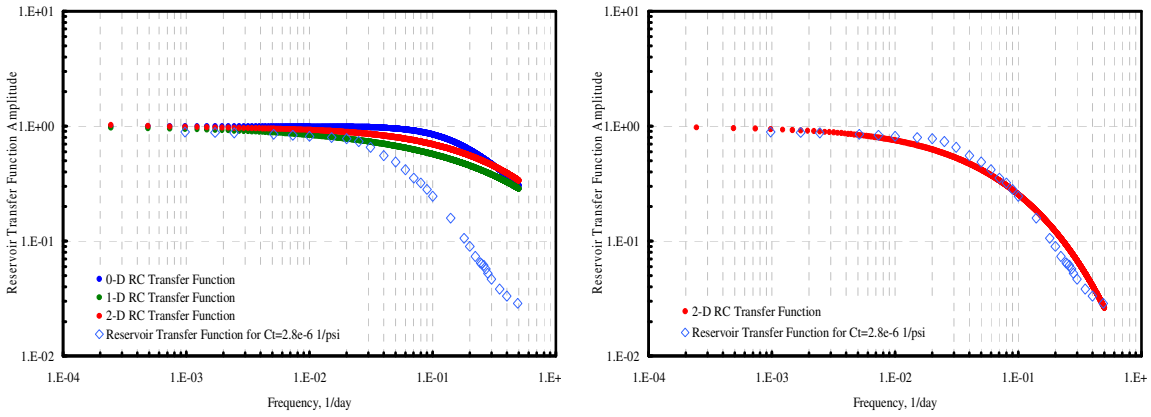

Figure 4.9— Comparison between RCTF and RTF for IDC=4.06E-01 sec/m^2 when (a) *RC*=4.06e-1 sec/m^2 (b) *RC*=3.22e+0 sec/m^2.

There is a poor fit between RTF and any of the RC models when $RC = \phi\mu C_t/k$ (**Fig. 4.9a**). For this case, the total fluids production is dominated by water production because water breaks through around 500 days. Thus, for a better fit, the *RC* value needs to be modified since most of the production is controlled by the endpoint effective permeability of 22.5 md. An additional modification is done on compressibility value by increasing it to 5e-6 1/psi, which is the water compressibility factor. As result of the comparison, the 2D RC model is selected as the best descriptive analytical solution possible (**Fig. 4.9b**).

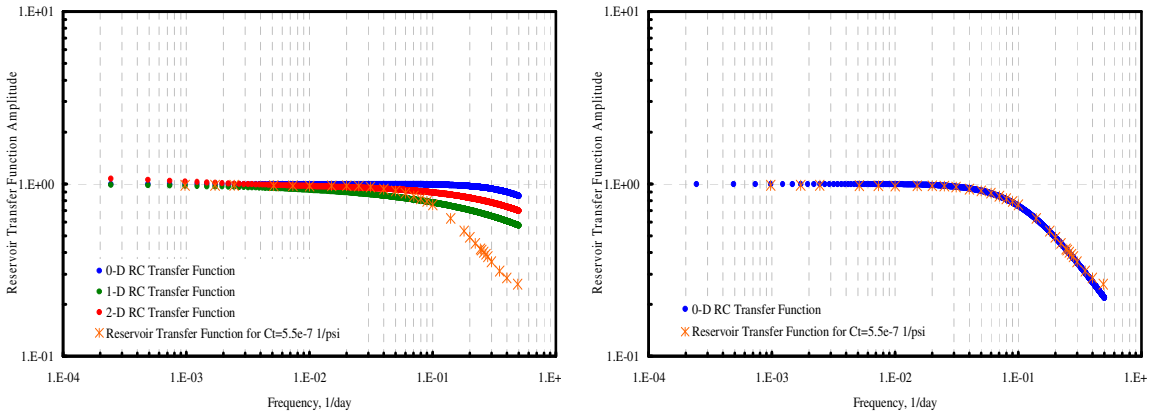

Figure 4.10— Comparison between RCTF and RTF for IDC=7.98E-02 sec/m^2 when (a) *RC*=7.98e-2 sec/m^2 (b) *RC*=6.44e-1 sec/m^2.

In **Figs. 4.10a** and **4.11a,** the results of the least and the most compressible system show what happens when we change the IDC of the reservoir system from 7.98e-2 to 7.98e-1 sec/m^2. For each system, we get very poor matches when $RC = \phi\mu C_t/k$. Since water production dominates the total fluids production, we make the similar modifications as we did in the previous case and reach succesful the matches in **Figs. 4.10b** and **4.11b**. In both cases, matches are very good and the modifications that we did because of the major water production make sense. The only difference between the cases is the type of the analytical solution that matches the RTF. In the least compressible case, it is the 0D model; on the other hand, it is the 2D model that gives the best match in the most compressible case. This application supports the result that we end up with the water-only case. As IDC increases, the accumulation in the reservoir increases; thereby, the heterogeneity of the displacement and the attenuation in the high-frequency components increase. Hence, 2D sophisticated solution becomes more descriptive for fluid flow identification in compressible reservoir models.

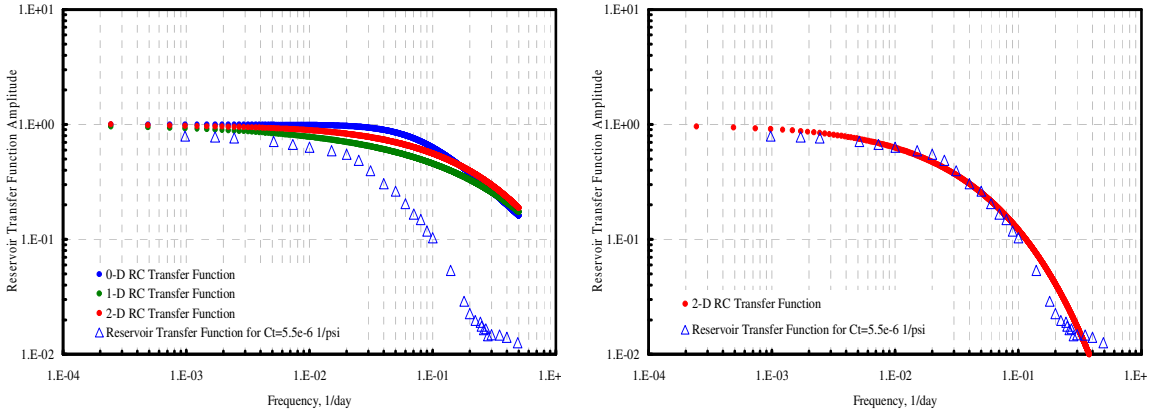

Figure 4.11— Comparison between RCTFs and RTFs for IDC=7.98e-1 sec/m^2 when (a) RC=7.98e-1 sec/m^2 (b) RC=6.44e+0 sec/m^2.

In this application, we modified the IDC values by switching the parameters from the total compressibility and the absolute permeability values to that of the water phase. As result of these modifications, we calculated the "estimated" IDC values; hence the "estimated" diffusivity parameters in **Table 4.6**.

Table 4.6— Interwell connectivity parameters estimated from spectral analyses in the dead oil and water production case. Modifications that we made to the RC coefficient led us to the estimated values of IDC and ϕ/k.

C_t 1/psi **Fig. 4.8**	IDC sec/m^2 **Fig. 4.9-11**	*RC* sec/m^2	RC Model	Estimated IDC sec/m^2	Ct.μ cp/psi **Table 4.5**	Estimated ϕ/k 1/md
5.50E-07	7.98E-02	6.44E-01	0D	6.44E-01	5.50E-07	8.08E-03
2.80E-06	4.06E-01	3.22E+00	2D	3.22E+00	2.80E-06	7.93E-03
5.50E-06	7.98E-01	6.44E+00	2D	6.44E+00	5.50E-06	8.08E-03

4.4.2 Dry Gas and Water Production Case

We performed another application on two-phase production in a reservoir that has a gas cap. We used the reservoir parameters and the relative permeability curves shown in **Table 4.7** and **Fig. 4.12**, respectively. In this application, we investigated the effect of free gas production on transfer functions. We reduced the injection rates by a factor of 10 from those of the base case.

Fig. 4.13 illustrates RTFs produced from three different total compressibility values. Basically, we kept the gas compressibility constant around 1e-5 1/psi and changed water compressibility to 1e-5, 5e-6 and 1e-6 1/psi. Water BT takes place around 500 days out of 4096 days. The range of IDC that we applied in this case is 2.3e-1 and 4.64e-1 sec/m^2.

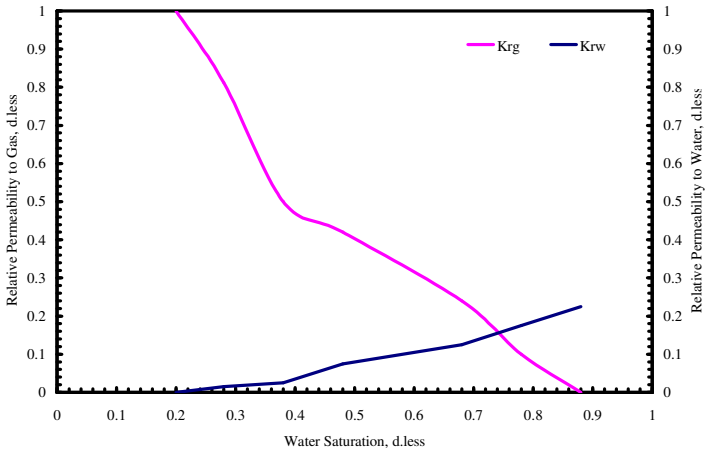

Figure 4.12—Relative permeability curves used in dry gas and water production.

Table 4.7—Reservoir parameters used for dry gas and water production.

Production phase	water, dry gas	
ϕ	0.1	d.less
k_x, k_y	100	md
k_z	1	md
μ_w	1	cp
B_w	1.01	RB/STB
C_w	1.00E-05 5.00E-06 1.00E-06	1/psi 1/psi 1/psi
μ_g	0.01	cp
B_g	0.96	RCF/SCF
C_g	1.00E-05	1/psi
C_f	1.00E-08	1/psi
S_{gir}	0.12	d.less
S_{wc}	0.2	d.less
BHP @producer	250	psi
Initial pressure	1470	psi
Duration	4096	days

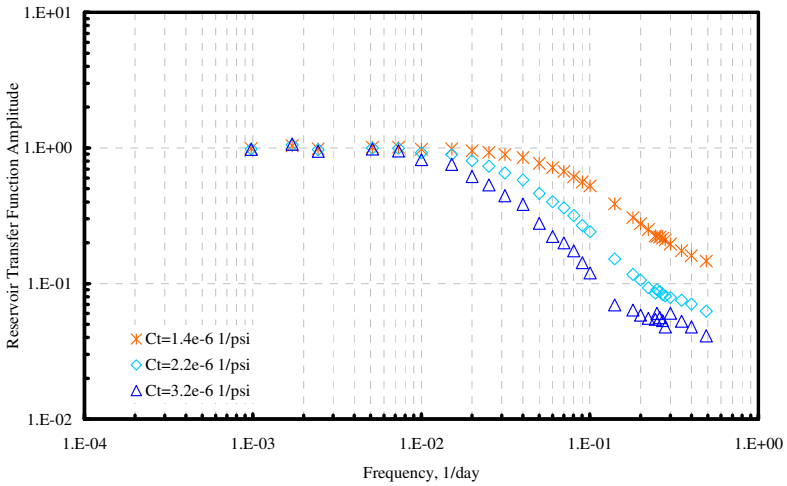

Figure 4.13—RTFs for dry gas and water production under various compressibility values.

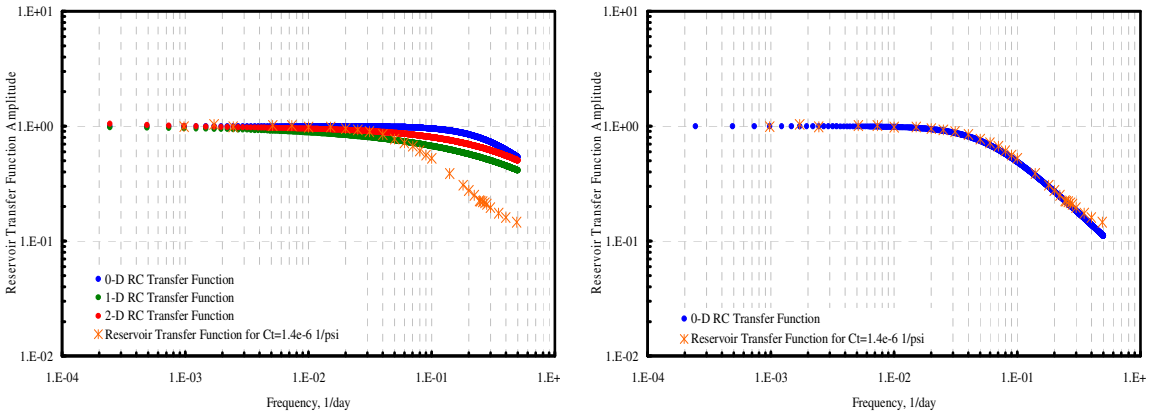

Figure 4.14— Comparison between three RCTFs and RTF for IDC=2.03e-1 sec/m^2 when (a) RC=2.03e-1 sec/m^2 (b) RC= 1.16e+0sec/m^2.

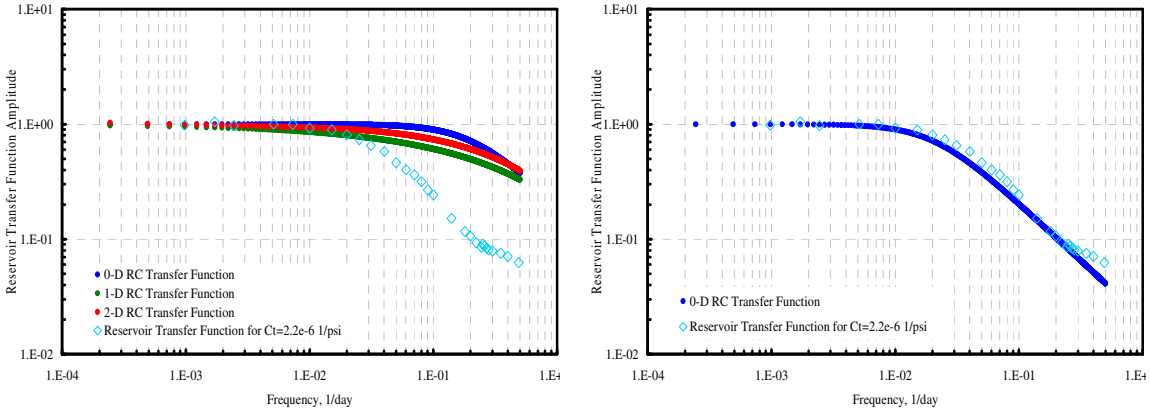

Figure 4.15— Comparison between three RCTFs and RTF for IDC=3.19E-01sec/m^2 when (a) *RC*=3.19e-1 sec/m^2 (b) *RC*=3.15e+0 sec/m^2.

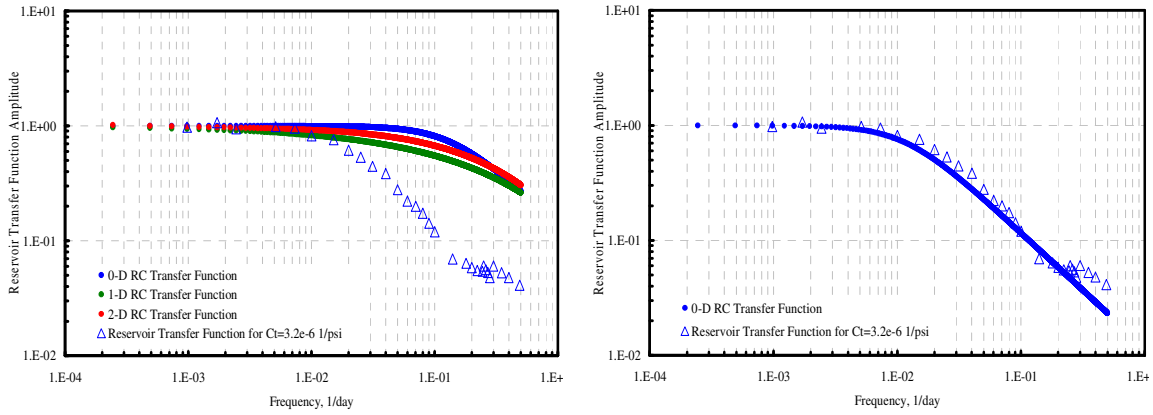

Figure 4.16— Comparison between three RCTFs and RTF for IDC=4.64e-1 sec/m^2 when (a) *RC*=4.64e-1 sec/m^2 (b) *RC*=5.58e+0 sec/m^2

In **Figs. 4.14a, 4.15a** and **4.16a**, we compare each RCTF with three analytical solutions to pick one of them as the best representative of the reservoir behavior. However, none of them fits the RTF for the particular IDC. Therefore, we applied similar modifications, as we did in the previous dead oil and water production case. As results of these modifications, we picked the 0D model as the best analytical solution that identifies the reservoir in the dry gas and water production case (**Figs. 4.14b, 4.15b** and **4.16b**).

We summarize the results from this application in **Table 4.8**. Similarly, we adjusted the *RC* coefficient of each analytical solution and calculated the "estimated" values of IDC to infer the connectivity in terms of ϕ/k. Finally, estimated results show that one can also understand that higher the compressibility in the reservoir; more difficult the reservoir fluid recovered by the injected water due to higher values of ϕ/k. Also, we show that 0D analytical solution is successful in fitting the reservoir behavior even at high compressibility values unlike the previous cases.

Table 4.8— Results of the interwell connectivity inferred from the dry gas and water production case. Higher the compressibility, lower the interwell connectivity parameters are obtained.

C_t 1/psi **Fig. 4.13**	IDC sec/m^2 **Fig. 4.14-16**	*RC* sec/m^2	RC Model	Estimated IDC sec/m^2	Ct.μ cp/psi **Table 4.7**	Estimated ϕ/k 1/md
1.40E-06	2.03E-01	1.16E+00	0D	1.16E+00	1.40E-06	5.71E-03
2.20E-06	3.19E-01	3.15E+00	0D	3.15E+00	2.20E-06	9.87E-03
3.20E-06	4.64E-01	5.58E+00	0D	5.58E+00	3.20E-06	1.20E-02

4.5 Dissolved Gas Production Around the Wellbore

We investigate if we can establish the similar analogy between RC networks and reservoir behavior when dissolved gas is produced around the wellbore due to the drop of reservoir pressure below saturation pressure.

We used the standard reservoir geometry and reduced the injection rates by a factor of 10 given the reservoir parameters in **Table 4.9** and the relative permeability curves in **Fig. 4.17**.

In this case, we applied different varieties of compressibility factor values to indicate the effects of both very high and very low compressibility effects. (**Table 4.10**) In total, we simulated 6 simulation models under the conditions stated in **Table 4.9**. Gas evolution around the wellbore is shown by saturation maps, which are located in Appendix B. Water breakthrough (BT) occurs around 345 day. Oil and dissolved gas production is performed up until BT. After BT, water production dominates the total fluids production. Although free gas production is not included in the application, dissolved gas production around the wellbore is available at very small values from the gas saturation maps.

Table 4.9—Reservoir parameters used for the simulated reservoir model.

Production phase	water, live oil, dissolved gas	
ϕ	0.1	d.less
k_x, k_y	100	md
k_z	1	md
μ_w	1	cp
B_w	1.01	RB/STB
C_w (when $C_{o\_undersaturated}$=1e-6 1/psi)	1.00E-06	1/psi
	1.00E-05	1/psi
	5.00E-06	1/psi
$\mu_{o\ undersaturated}$	0.94	cp
$B_{o\_undersaturated}$	Appendix B	
$C_{o\_undersaturated}$ (when C_w=1e-6 1/psi)	1.00E-06	1/psi
	5.00E-06	1/psi
	1.00E-05	1/psi
	5.00E-05	1/psi
C_f	1.00E-06	1/psi
S_{wc}	0.35	d.less
S_{or}	0.35	d.less
BHP @producer	3500	psi
Initial pressure	4100	psi
Saturation pressure	4000	psi
Duration	4096	days

Table 4.10—Compressibility factors used for the simulated reservoir model.

	Simulation Run #	Oil Compressibility Factor, 1/psi	Water Compressibility Factor, 1/psi	Total Compressibility Factor, 1/psi
Part 1	1	1.00E-06	1.00E-06	1.70E-06
	2	1.00E-06	5.00E-06	3.10E-06
	3	1.00E-06	1.00E-05	4.85E-06
Part 2	4	5.00E-06	1.00E-06	3.10E-06
	5	1.00E-05	1.00E-06	4.85E-06
	6	5.00E-05	1.00E-06	1.89E-05

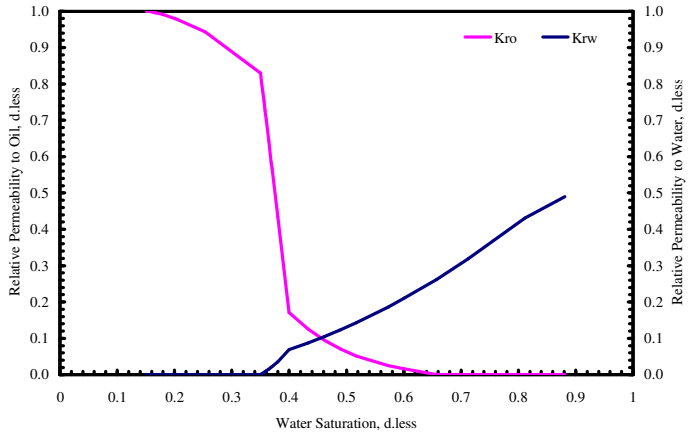

Figure 4.17—Relative permeability curves used in the reservoir simulation.

We present the effect of the dissolved gas production in terms of TF in **Fig. 4.18**. Each one of the functions represents a simulation run when oil and water compressibility factor is set to a specific value. We can show the simulations runs in two parts (**Table 4.9**):

- *Part 1*: C_o is equal to 1e-6 1/psi. C_w is changed to 1e-6, 5e-6, 1e-6 1/psi.
- *Part 2*: C_w is equal to 1e-6 1/psi. C_o is changed to 1e-6, 5e-6, 1e-5, 5e-5 1/psi.

As a result of this sensitivity analysis, we investigate the variations in attenuation of each simulation model due to the differences in total compressibility factors and the heterogeneity of the systems due to the dissolved gas production.

The most compressible case is when we set the oil compressibility to 5e-5 1/psi. Ripples at the stopband are at their highest level in this case. The least compressible system is when both oil and water compressibility values are set to 1e-6 1/psi.

Our objective is to understand if we can still use RCTFs to identify an RTF when dissolved gas production occurs around the wellbore. Obviously, the dissolved gas production does not mask the main signal in the spectrum due to the useful presentation of the main signal that consists of 30 frequency components. Hence, we can still apply our method to infer connectivity parameters even though the displacement

process gets more complicated by adding the dissolved gas into the producing phases. Moreover, we can quantify the heterogeneity of the system only by the *RC* coefficient of RCTF that fits the particular RTF. Because we have experienced from the spectral analysis so far that higher the *RC* coefficient, more heterogeneous the system is.

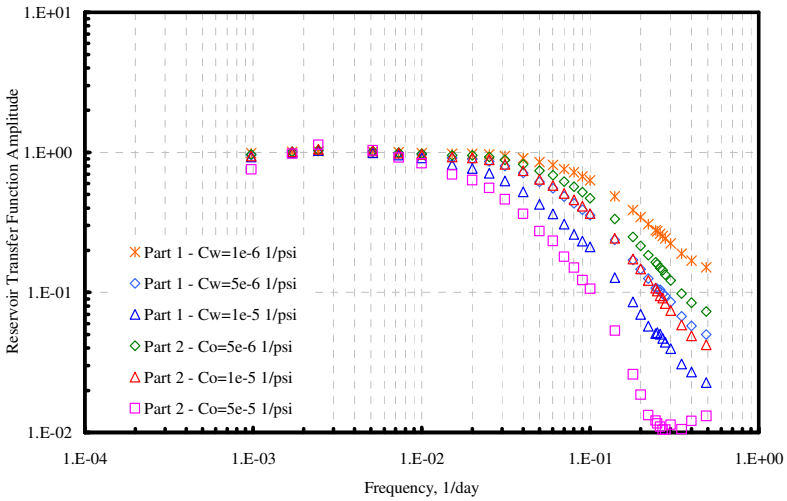

Figure 4.18— RTFs produced from the live oil and water production simulations for various compressibility values.

We display the comparisons of RTFs with the correspondent RCTF in **Figs. 4.19, 4.20** and **4.21**. As we have performed in the previous applications, we compare three RCTFs, which we calculated by the exact diffusivity parameters, with the RTF (**Figs 4.19a**, **4.20a**, and **4.21a**). If none of three RC models fit the particular RTF, we adjust the *RC* coefficient to fit the reservoir behavior (**Figs 4.19b**, **4.20b**, and **4.21b**). Then, we assign the adjusted *RC* coefficient to the IDC to compute the estimated values of interwell connectivity information, which is ϕ/k. (**Table 4.11**)

We show that 0D RC model fits the least compressible systems perfectly well (**Fig.4.19b**), as we have experienced previously, when we adjust the RC coefficient to 8.99e-1 sec/m^2.

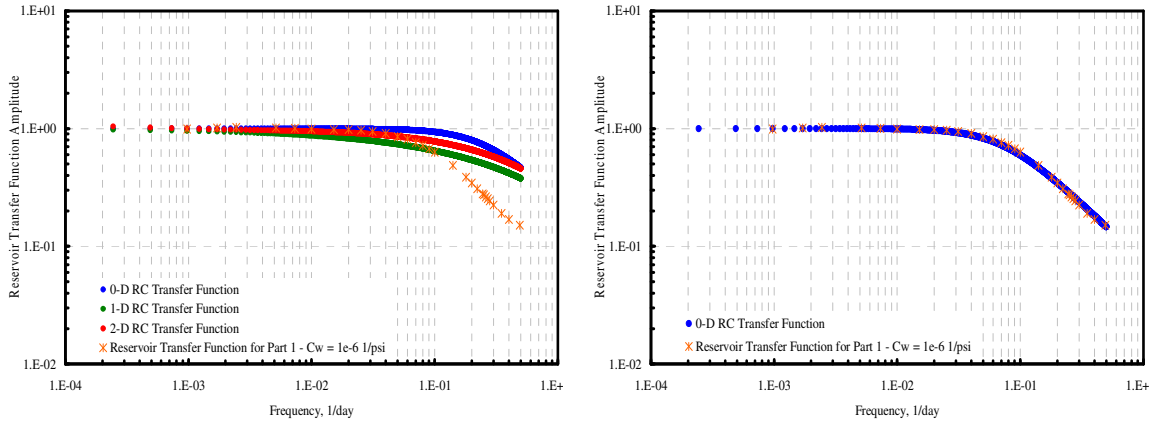

Figure 4.19— Comparison between RTF for IDC=2.47e-1 sec/m^2 and RCTFs when (a) *RC*=2.47e-1 sec/m^2 (b) *RC*=8.99e-1 sec/m^2.

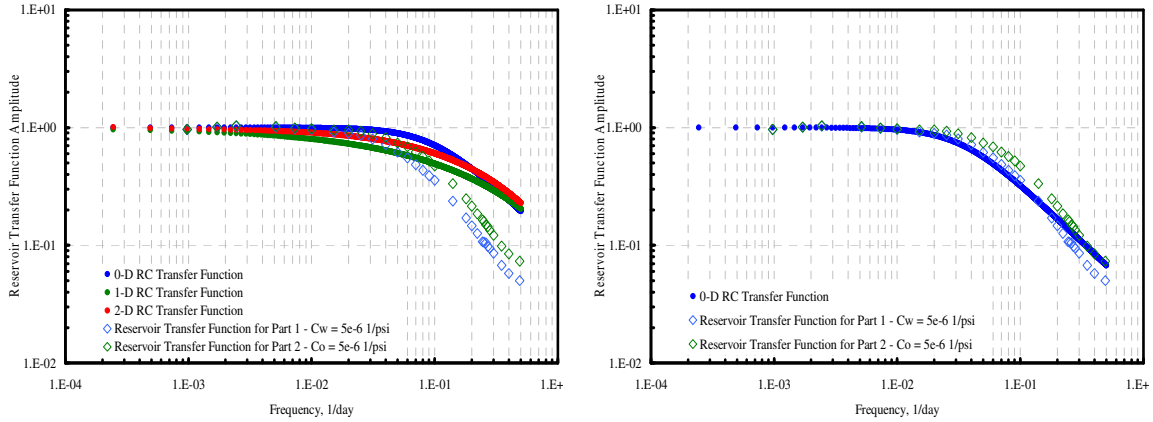

Figure 4.20— Comparison between RTF for IDC=4.5e-1 sec/m^2 and RCTFs when (a) *RC*=4.5e-1 sec/m^2 (b) *RC*=1.92e+0 sec/m^2.

Although their total compressibility factors are same (C_t=3.1e-6 1/psi and 4.85e-6 1/psi, respectively), reservoir behavior in **Figs. 4.20a** and **4.21a** show different results. The reason of this situation is the water production that dominates the total fluids production and has different water compressibility values in each run (**Table 4.10**). However, the RCTF that fits one RTF can not fit the other RTF; therefore, the fits that we obtain in these practices will not be perfect to infer connectivity parameters (**Figs. 4.20b** and **4.21b**), but they are very close to make estimations.

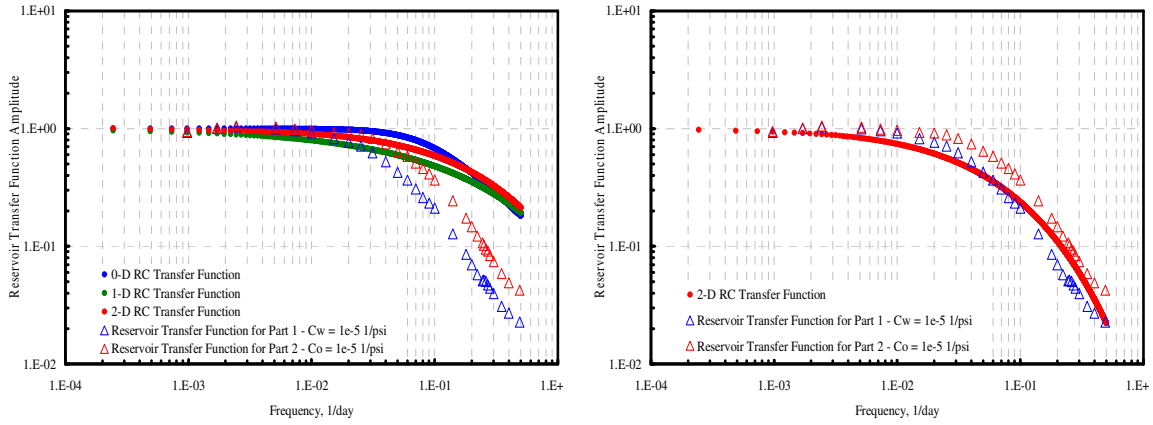

Figure 4.21— Comparison between RTF for IDC=7.03e-1 sec/m^2 and RCTFs when (a) *RC*=7.03e-1 sec/m^2 (b) *RC*=3.14e+0 sec/m^2.

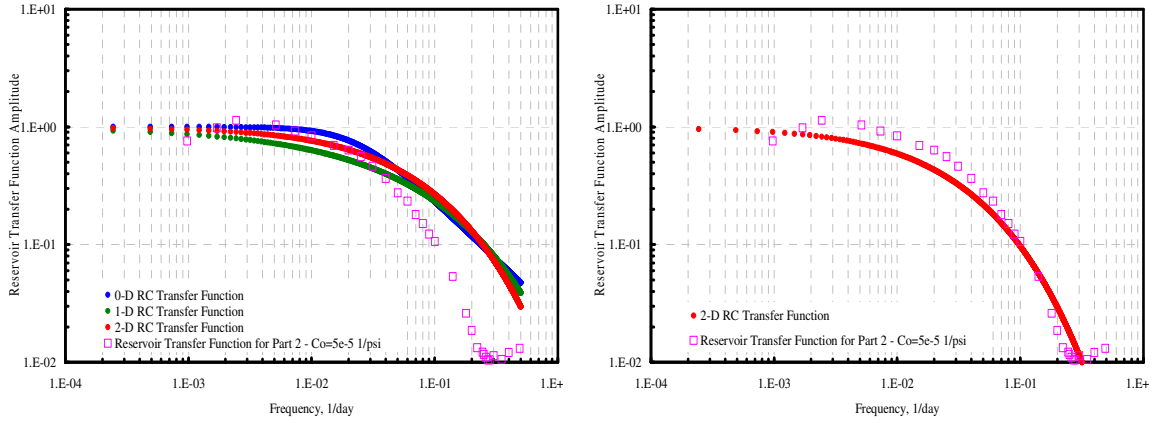

Figure 4.22— Comparison between RTF for C_t=1.89e-5 1/psi and RCTFs when (a) *RC*=2.74e+0 sec/m^2 (b) *RC*=6.89e+0 sec/m^2.

Figs. 4.22a and **4.22b** present the most compressible system that we applied in this case. It is the most heterogeneous case of all applications and cases that we have practiced so far. We have already experienced that we can see the heterogeneity of the displacement process by looking at the degree of the attenuation of RTF in its high frequencies. In this case, stopband also exists by forming ripples and making it hard to fit an RCTF. As we stated, we do not include the ripples of a stopband in the

quantitative analysis. After adjusting the *RC* coefficient to obtain a better match in **Fig 4.22b**, the fit to the RTF is good enough to make an estimation of the interwell connectivity parameters.

Finally, the results of the dissolved gas production around wellbore indicates that except for the least compressible system, all models have a good enough match with an RCTF to make estimations. The least compressible system has the best match; hence it offers the most reliable interwell connectivity information. In other words, we can not make perfect matches and perfect estimations when we handle more complicated displacement processes as in **Figs. 4.20**, **4.21**, and **4.22**. **Table 4.11** summarizes the results obtained from this application displaying the estimated IDC from the analogy and the interwell connectivity information in the last column.

Table 4.11—Interwell connectivity inferred from the dissolved gas production case.

Sim Run #	Ct 1/psi **Fig. 4.18**	IDC sec/m^2	*RC* Coefficient sec/m^2	RC Model	Estimated IDC sec/m^2	Ct.μ cp/psi **Table 4.10**	Estimated ϕ/k 1/md
1	1.70E-06	2.47E-01	8.99E-01	0D	8.99E-01	1.70E-06	3.65E-03
2	3.10E-06	4.50E-01	1.92E+00	0D	1.92E+00	3.10E-06	4.27E-03
3	4.85E-06	7.03E-01	3.14E+00	2D	3.14E+00	4.85E-06	4.46E-03
4	3.10E-06	4.50E-01	1.21E+00	1D	1.21E+00	3.10E-06	2.69E-03
5	4.85E-06	7.03E-01	2.42E+00	2D	2.42E+00	4.85E-06	3.44E-03
6	1.89E-05	2.73E+00	6.89E+00	2D	6.89E+00	1.89E-05	2.52E-03

4.6 Conclusions

1. We performed applications only on single-phase (water-only) production and two-phase production under various total compressibility factors including the dissolved gas evolution around wellbore application.

2. We successfully matched RTFs with the correspondent RCTFs in the single-phase production results with no modification on the *RC* coefficient. Therefore, the estimated IDC is equal to the original IDC.

3. When we increase the total compressibility to 5e-5 1/psi in the single-phase production, a stopband, besides a passband and a transition band, appears along with some ripples at high frequency values. In this case, we used 2D RC model to identify the reservoir behavior. 2D RC model is more descriptive when *RC* coefficient increases up to 7.25 sec/m^2.

4. In the two-phase dead oil and water production, we obtained the best result from the least compressible reservoir model when water compressibility is set to 1e-6 1/psi. Lumped 0D RC model fits perfectly to the RTF when we modified the *RC* coefficient due to the relative permeability to water and the water compressibility factor. In more compressible systems when we set the water compressibility to 1e-5 and 5e-6 1/psi, 2D RC model captures RTF better; however the results are not as accurate as the one in the least compressible reservoir model.

5. In the two-phase dry gas and water production, we again obtained the most reliable analogy from the least compressible reservoir model when total compressibility factor is 1.4e-6 1/psi. In that case, unlike the other applications, 0D RC model fits RTFs for all compressibility values. However, the results are all good enough to make estimations for interwell parameters.

6. As a result of the dissolved gas production around the wellbore application, we can state that dissolved gas production that has been excluded from the interwell connectivity studies so far, can be analyzed by our method to infer interwell connectivity parameters. However, the results are not as good as the liquid production cases.

7. We kept the fits of the models to RTFs to only visual assessments rather than applying statistical methods such as coefficient of determination (r^2) to prove how close the fits are. The reason to that is these applications are not used systematically in a project that provides very sensitive information. The applications are only representative of a proof of concept that might be a beginning of a more detailed study.

CHAPTER V

SUMMARY, CONCLUSIONS AND RECOMMENDATIONS FOR FUTURE WORK

5.1 Summary

This study is a proof of concept, which infers IDC parameters between an injector and a producer in a waterflooded homogenous reservoir by utilizing only the injection and the production flow rate data. The method requires frequency domain analysis of the flow rate data by using FT's and an analogy between RC networks and reservoirs that provides analytical solutions to the transmission line equation.

Hypothetical reservoir models are simulated in the validation part to investigate under which conditions the method works. Ultimately, dissolved gas production around wellbore is modeled to see if the spectrum of the reservoir flow rate data is masked by the dissolved gas production, so interwell connectivity inference is possible by this method.

In Chapter I, the objectives of the study, the analogy between an RC network and a reservoir are explained and a wide range of literature reviews is depicted. The analogy between an RC device and a reservoir is already available in literature by Bruce (1943). He introduced the analogy between these two media based on a tank model by the following material balance formulas:

$$q_{net} = V_p c_t \frac{dp}{dt} \quad (5.1)$$

$$i_{net} = C_E \frac{dv}{dt} \quad (5.2)$$

Depending on Bruce's work and the similarity between diffusivity equation and transmission line equation as stated respectively in Eqs. 5.3 and 5.4, the analogy in this method is based on the relationship between the coefficients in Eq.5.5.

$$\frac{\partial^2 p}{\partial z^2} = \frac{\phi \mu c_t}{k} \frac{\partial p}{\partial t} \quad \text{.....(5.3)}$$

$$\frac{\partial^2 v}{\partial z^2} = RC \frac{\partial v}{\partial t} \quad \text{.....(5.4)}$$

$$\frac{\phi \mu c_t}{k} \sim RC \quad \text{.....(5.5)}$$

Analytical solutions of RC network that are derived in 3 dimensional choices are used to identify the reservoir behavior through the use of transfer functions. The analogy for 1D and 2D dimensional models between two coefficients in Eq. 5.5 is used to define the IDC and thereby, the ranges of porosity and permeability values to infer interwell connectivity.

In Chapter II, 0D, 1D and 2D analytical solutions to the transmission line equation are shown and RCTF'ss are introduced. The results of the analytical solutions are represented in terms of RCTF'ss which are stated in the following equations.

$$H_{0D}(f) = \frac{1}{1 + j\omega RC} \quad \text{.....(5.6)}$$

$$H_{1D}(z) = e^{-z\sqrt{\frac{\omega RC}{2}}} e^{-zj\sqrt{\frac{\omega RC}{2}}} \quad \text{.....(5.7)}$$

$$H_{2D}(r) = r\sqrt{j\omega RC}\,\mathrm{K}_1\left[\sqrt{j\omega RC}\,r\right] \quad \text{.....(5.8)}$$

Three RCTF'ss are calculated given the *RC* coefficient and the interwell distance between the well pair. *RC* coefficient is calculated from the relationship stated in Eq. 5.5.

In Chapter III, frequency domain analyses performed on reservoir flow rate data are shown and RTFs of various discrete time series are introduced. A specific injection flow rate is generated based on 30

frequencies to produce a very accurate RTF to be used in further analysis to maintain an analogy with a RCTF.

In Chapter IV, hypothetical reservoir models created in Eclipse are used to validate the method through the use of RC and RTF's, which are explained separately in Chapters II and III, respectively. Cases are applied on single and two-phase production. Ultimate goal was to investigate if dissolved gas production around wellbore masks the RTF spectrum and destroy the main signal to be analyzed.

5.2 Conclusions

The analogy between RC networks and reservoirs are applied on hypothetical cases that are modeled in black oil simulator. No real field data is used to validate the results. The concluding remarks from this study are as follows:

1. Using only injection and production flow rate data in frequency domain with the transfer functions and an analogy to the RC networks is a multi-disciplinary work. It provides an estimation of connectivity information between a well pair in a homogenous porous media.

2. This method indicates that higher the RC coefficient determined from an analogy between an RC network and a reservoir, higher the heterogeneity of the displacement process. Thus, the *RC* coefficient yielded from the analogy provides a quantitative approach to re-estimate the IDC, which results in a alternative way to infer interwell connectivity.

3. In addition to the tank model, which is used as a solution of the analog RC devices in the literature, 2D RC analytical solutions can also be applied to perform analogy between electrical flow and fluid flow.

4. This analogy is proven to be applicable to provide quantitative results only in a simple reservoir where the assumptions of the analytical solutions are nearly met. The analog RC network models are able to identify the RTF's only if the following conditions are provided:
   - Homogeneous, isotropic porous media

- Small compressibility values around 1e-6 1/psi
- Sinusoidal injection rate which has enough frequencies to construct the RTF.

5. Although the parameters of the hypothetical reservoir models do not meet the analytical solution parameters in two-phase production applications, deviations from the assumptions can be tolerated in the following applications performed in this study to estimate diffusivity parameters:
   - Dead oil + water production
   - Dry gas + water production
6. Dissolved gas production incorporates huge heterogeneity to the reservoir system; therefore the estimations provided from the analogy result poor predictions.
7. For high compressibility values in a reservoir, this method provides qualitative information based on the ripples appearing in the stopbands. This might be useful in making qualitative comparisons between different reservoir models.
8. Injection rate based on 30 particular frequency components is very useful in maintaining a main signal in frequency domain while performing spectral analysis on flow rate data, even in noisy processes.
9. Fourier transforms are very successful for the purposes of this study in terms of extracting the main signal at average amplitudes.
10. The analytical solutions are unable to reflect the behavior of a stopband in a RTF. The ripples that appear in high frequency components are excluded from the quantitative analyses. However, they can be used to provide qualitative information.

5.3 Recommendations for Future Work

This method is applied on very simple hypothetical reservoir models to show a proof of principle between a single well pair. The analogies are based on the matches between RC and reservoir TF's only visually.

The study can be extended over simple reservoir geometries for small compressibility values on multiple well pairs along with weighting averages. In this case, the matches between transfer functions can be evaluated statistically in more detail and the estimated reservoir parameters from multiple well pairs can be cross plotted to infer the connectivity.

NOMENCLATURE

C_E	=	Capacitance, μfarads
V_p	=	Pore volume, bbl
c_t	=	Total compressibility, 1/psi
q_1	=	Flow rate in, bbl/day
q_2	=	Flow rate out, bbl/day
p	=	Pressure, psi
t	=	Time, day
i_1	=	Current in, μA
i_2	=	Current out, μA
z	=	Point in space, ft
ϕ	=	Porosity, d.less
μ	=	Viscosity, cp
k	=	Permeability, md
v	=	Voltage, volts
R	=	Resistance, ohms
C	=	Capacitance, farads
$Y(f)$	=	FT of the production rate
$X(f)$	=	FT of the injection rate
$H(f)$	=	Transfer function of the reservoir
$f(t)$	=	a given arbitrary function
a_0	=	the constant term in the Fourier series approximation
a_n	=	a coefficient in the Fourier series approximation
b_n	=	a coefficient in the Fourier series approximation
$s_N(\mathrm{t})$	=	n^{th} partial sum of the Fourier series approximation
N	=	degree of polynomial
n	=	1,2…N
t	=	time, sec
f	=	Frequency, 1/sec
V_{out}	=	Voltage at the receiving end, volts
V_{in}	=	Voltage at the sending end, volts
ω	=	Angular frequency, radian/sec
j	=	Imaginary unit

A = Constant coefficient

j = Imaginary unit

r = radius, ft

T = Temperature, K

κ = Heat diffusivity

κ = Heat diffusivity coefficient

K = Thermal conductivity, W/mK

ρ = Density, kg/m^3

c = Specific heat, J/gK

$F(z,t)$ = Heat flux or current flux

$F(z,t)$ = Flux at the receiving end of the RC network (output)

$F(0,t)$ = Flux at the sending of the RC network (input)

$w(n)$ = Blackman window function

N = Width of the window

n = Integer with values $0 \leq n \leq N - 1$

$K_0(r)$ = Modified Bessel function of the second kind, zero order

$K_1(r)$ = Modified Bessel function of the second kind, first order

$H_{0D}(f)$ = Transfer function of a lumped RC network

$H_{1D}(z)$ = Transfer function of the 1D RC network

$H_{2D}(f)$ = Transfer function of the 2DRC network

REFERENCES

Al-Yousef, A.A., Gentil, P., Jensen, J.L., and Lake, L.W.: "A Capacitance Model To Infer Interwell Connectivity From Production and Injection Rate Fluctuations," paper SPE 95322 presented at the 2005 SPE Annual Technical Conference and Exhibition, Dallas, Texas, 9-12 October.

Albertoni, A.: "Inferring Interwell Connectivity from Well Rate Fluctuations in Waterfloods", M.S. thesis, U. of Texas at Austin, Austin, Texas (2002).

Albertoni, A., and Lake, L.W.: "Inferring Interwell Connectivity Only From Well-Rate Fluctuations in Waterfloods," paper SPE 75225 presented at the 2002 SPE/DOE Improved Oil Recovery Symposium, Tulsa, Oklahoma, 13-17 April.

Bruce, W.A.: "An Electrical Device for Analyzing Oil Reservoir Behavior" *Trans*, AIME, p.113-124, 1943.

Carslaw, H.S., and Jaeger, J.C.: *Conduction of Heat in Solids,* 2nd edition, Oxford University Press, New York (1986).

De Sant Anna'Pizzaro, J.O.: *Estimating Injectivity and Lateral Autocorrelation in Heterogeneous Media*, Ph.D dissertation, U. of Texas at Austin, Austin, Texas (1999).

Everitt, W.L., and Anner, G.E.: *Communication Engineering*, 3rd edition, McGraw Hill, New York (1956).

Harman, T.L., Dabney, J., and Richert, N.: *Advanced Engineering Mathematics with Matlab*, Brooks/Cole, California (2000).

Heffer, K.J., Fox, R.J., and McGill, C.A.: "Novel Techniques Show Links Between Reservoir Flow Directionality, Earth Stress, Fault Structure and Geomechanical Changes in Mature Waterfloods," paper SPE 30711 presented at the 1995 SPE Annual Technical Conference and Exhibition, Dallas, Texas, 22-25 October.

Hollaender, F., Hammond, P.S., and Gringarten, A.C.: "Harmonic Testing for Continuous Well and Reservoir Monitoring," paper SPE 77692 presented at the 2002 SPE Annual Technical Conference and Exhibition, San Antonio, Texas, 29 September -12 October.

Irwin, J.D.: *Basic Engineering Circuit Analysis*, 7th edition, John Wiley & Sons, New York (2002).

Jansen, F.E., and Kelkar, M.G.: "Application of Wavelets to Production Data in Describing Inter-Well Relationships," paper SPE 38876 presented at the 1997 SPE Annual Technical Conference and Exhibition, San Antonio, Texas, 5-8 October.

Johnson, C.R., Greenkorn, R.A., and Woods, E.G.: "Pulse-Testing: A New Method for Describing Reservoir Flow Properties Between Wells," paper SPE 1517 presented at SPE 41st Annual Fall Meeting in 1966, Dallas, Texas, 2-5 October.

Kreyszig, E.: *Advanced Engineering Mathematics*, 8th edition, John Wiley & Sons, New York (2000).

Kuo, C.H.: "Determination of Reservoir Properties from Sinusoidal and Multirate Flow Tests in One or More Wells," paper SPE 3265 presented at SPE 46th Annual Fall Meeting in 1971, New Orleans, Louisiana, 3-6 October.

Lee, J., Rollins, J.B., and Spivey, J.P.: *Pressure Transient Testing*, Textbook Series, *SPE*, Vol. 9, Richardson, Texas (2003).

Muskat, M.: *Physical Principles of Oil Production*, McGraw Hill, New York (1949).

Panda, M.N. and Chopra, A.K.: "An Integrated Approach to Estimate Well Interactions," paper SPE 39563 presented at the 1998 SPE India Oil and Gas Conference and Exhibition, New Delhi, 17-19 February.

Refunjol, B.T.: "Reservoir Characterization of North Buck Draw Field Based on Tracer Response and Production/Injection Analysis", M.S. thesis, U. of Texas at Austin, Austin, Texas (1996).

Rosa, A.J and Horne, R.N.: "Reservoir Description by Well-Test Analysis by Use of Cyclic Flow-Rate Variation," paper SPE 22698 presented at the 1991 SPE Annual Technical Conference and Exhibition, Dallas, Texas, 6-9 October.

Smith, S.W.: *The Scientist and Engineer's Guide to Digital Signal Processing*, 2nd edition, California Technical Publishing, San Diego (1999).

Soeriawinata, T. and Kelkar, M.: "Reservoir Management Using Production Data," paper SPE 52224 presented at the 1999 SPE MidContinent Operation Symposium, Oklahoma City, Oklahoma, 28-31 March.

Wahl, W.L., Mullins, L.D., Barham, R.H., and Bartlett, W.R.: "Matching the Performance of Saudi Arabian Oil Fields With an Electrical Model," paper SPE 414 presented at SPE 37th Annual Fall Meeting in 1962, Los Angeles, California, 7-10 October.

APPENDIX A

FUNDAMENTAL KNOWLEDGE IN FOURIER TRANSFORMS

A.1 Fourier Series

Davis (1973) states that Fourier analysis is the decomposition of a signal into its harmonic constituents. A signal is composed of three parts: a linear trend in the average value of the signal, various periodic components and a random component. After removing the trend component, the remaining parts consist of a signal (periodic components) and noise (random components). One of the purposes of Fourier analysis is to extract the dominant periodic components.

As mentioned earlier, the purpose of Fourier analyses is to express an arbitrary function, *f(t),* as a linear combination of a set of *N* harmonic sine and cosine basis functions (Harman, 2000).

$$f(t) \approx \frac{a_0}{2} + \sum_{n=1}^{N} \left[a_n Cos(nt) + b_n Sin(nt) \right] = s_N(t) \,. \quad \text{.....(A.1)}$$

where $s_N(t)$ is the Fourier approximation to the function *f(t)* by using a trigonometric polynomial of degree *N* assuming *f(t)* is continuous on the interval [-π, π]. The constant term a_0 and the Fourier coefficients a_n and b_n in Eq. A.1 can be computed by Eqs A.2, A.3 and A.4 respectively for n=1,2…N.

$$a_0 = \frac{1}{\pi} \int_{-\pi}^{\pi} f(t)dt \,. \quad \text{.....(A.2)}$$

$$a_n = \frac{1}{\pi} \int_{-\pi}^{\pi} f(t)Cos(nt)dt \,. \quad \text{.....(A.3)}$$

$$b_n = \frac{1}{\pi} \int_{-\pi}^{\pi} f(t)Sin(nt)dt \,. \quad \text{.....(A.4)}$$

Applications of periodic functions can have periods other than 2π. Therefore, the following Eq. A.5 will be a representation that covers a period of *T*. If the given arbitrary function, *f(t)*, is periodic on the interval [-T/2, T/2] instead of [-π, π], the limits of integration for the Fourier series can be changed from [-π, π] by

rescaling the variable t as $2\pi t / T$. Then, the constant term a_0 and the coefficients a_n and b_n in Eqs. A.2, A.3 and A.4 need to be redefined to be able to make the new Fourier approximation to the function $f(t)$ on that given interval by the following expressions.

$$a_0 = \frac{2}{T}\int_{-T/2}^{T/2} f(t)dt \quad \text{.....(A.5)}$$

$$a_n = \frac{2}{T}\int_{-T/2}^{T/2} f(t)Cos(\frac{2n\pi t}{T})dt \quad \text{.....(A.6)}$$

$$b_n = \frac{2}{T}\int_{-T/2}^{T/2} f(t)Sin(\frac{2n\pi t}{T})dt \quad \text{.....(A.7)}$$

Therefore, the new approximation to the given arbitrary function which is continuous on the interval [-T/2, T/2] is as Eq. A.8 Since the sum contains an infinite number of terms, the equality sign in Fourier series expansions is used instead of the approximation sign.

$$f(t) = \frac{a_0}{2} + \sum_{n=1}^{\infty}\left[a_n Cos(\frac{2n\pi t}{T}) + b_n Sin(\frac{2n\pi t}{T})\right] \quad \text{.....(A.8)}$$

Assuming the variable t represents time, the function $f(t)$ repeats every T seconds (period) which means that the frequency of the series above is $f_0 = 1/T$, in cycles per second, or hertz. Eq. A.8 can be rewritten by incorporating f_0:

$$f(t) = \frac{a_0}{2} + \sum_{n=1}^{\infty}\left[a_n Cos(2\pi n f_0 t) + b_n Sin(2\pi n f_0 t)\right] \quad \text{.....(A.9)}$$

or

$$f(t) = \frac{a_0}{2} + \sum_{n=1}^{\infty}\left[a_n Cos(n\omega_0 t) + b_n Sin(n\omega_0 t)\right] \quad \text{.....(A.10)}$$

where

$$\omega_0 = 2\pi f_0 = \frac{2\pi}{T} \quad \text{.....(A.11)}$$

The first terms in sine and cosine functions, which are a_n and b_n, are called the fundamental components, the other terms are the harmonics with frequencies that are integer multiples of the fundamental component's frequency. When the Fourier series is used to approximate *f(t)*, the *f(t)* must be a continuous function of time.

Generally, the Fourier series of a periodic function with period *T* seconds contains the fundamental and numerous harmonics. The component magnitudes of the series allow the interpretation of the function in terms of its frequency spectrum. The plot of the magnitude of the frequency components is called the frequency spectrum, where the frequency components are spaced $f_0 = 1/T$ hertz apart from each other.

A.2 Fourier Transform

The FT is an extension of Fourier analysis to the analysis of non-periodic functions. In the analysis of such functions, the sum of the discrete frequencies must be replaced by an integral. Let the function *f(t)* be continuous in every piece for $-\infty < t < \infty$ and let $\int_{-\infty}^{\infty} |f(t)|\,dt$ exist so that the result is finite, then the FT of *f(t)* is as follows:

$$\mathbb{F}[f(t)] = F(i\omega) = \int_{-\infty}^{\infty} f(t) e^{-i\omega t}\,dt \quad \text{.....(A.12)}$$

where $F(i\omega)$ represents the frequency spectrum of *f(t)*. It may be complex even if *f(t)* is real. Thus, the magnitude $|F(i\omega)|$ is called the amplitude spectrum of $F(i\omega)$ (Kreyszig, 2000).

A.3 Discrete Fourier Transform

The Fourier series and the FT are applied to functions *f(t)* that are continuous and known for all values of *t*. However, Fourier analysis by computer requires a finite number of samples of *f(t)* (Kreyszig, 2000).

Typically, the signals are sampled at equally spaced points in time. As noted in previous sections, it is assumed that the function or a signal being analyzed is infinitely long in time when solving analytically.

Assume that a function *f(t)* is sampled at intervals $\Delta t=T_s$ seconds to create a set of *N* points. The length in time of the sampled signal is $(N-1)T_s$ seconds. The function at point *n* is denoted by *f(nTs)* for *n=0,…,N-1* values. The discrete Fourier transform (DFT) produces the frequency spectrum by the following formula:

$$F_k = F\left(\frac{k}{NT_s}\right) = \sum_{n=0}^{N-1} f\left(nT_s\right) e^{-i2\pi nk/N} \quad \text{.....(A.13)}$$

for $k=0,\ldots,N-1$.

As a result of applying the DFT, the *N* sample points of *f(t)* in the time domain produce *N* frequency components in the discrete spectrum spaced at intervals $f_s=1/(NT_s)$.

The DFT of a real function *f(t)* results with a complex number of F_k. Thus, the magnitude of the complex number is needed to be taken by the following equation:

$$\left|F(f)\right| = \sqrt{\left|F_r(f)\right|^2 + \left|F_i(f)\right|^2} \quad \text{.....(A.14)}$$

The algorithms that are used to calculate the DFT are called fast FT algorithms. Throughout the study of this proposed work, Matlab has been used for DFT calculations.

APPENDIX B

GAS SATURATION MAPS RELATED TO THE DISSOLVED GAS APPLICATION

Gas evolution around wellbore is modeled in reservoir models from 6 reservoir simulation runs which are summarized in **Table B.1**. Varieties of oil and water compressibility factors are used to produce these saturation maps. Regarding the change in oil compressibility factors, formation volume factor versus pressure figure is displayed in **Fig. B.1**. According to the following **Figs. B.2 – B.7,** it is shown that gas evolution around the wellbore decreases by the increasing compressibility factor of oil.

Table B.1—Summary of simulation runs in dissolved gas production case.

Simulation Run #	Oil Compressibility Factor, RB/STB	Water Compressibility Factor, RB/STB	Total Compressibility Factor, RB/STB
1	1.00E-06	1.00E-06	1.70E-06
2	1.00E-06	5.00E-06	3.10E-06
3	1.00E-06	1.00E-05	4.85E-06
4	5.00E-06	1.00E-06	3.10E-06
5	1.00E-05	1.00E-06	4.85E-06
6	5.00E-05	1.00E-06	1.89E-05

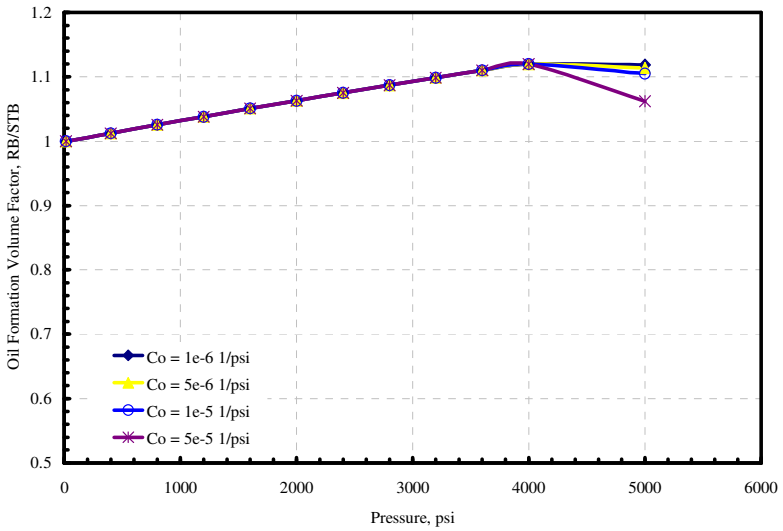

Figure B.1—Oil formation volume factor versus pressure.

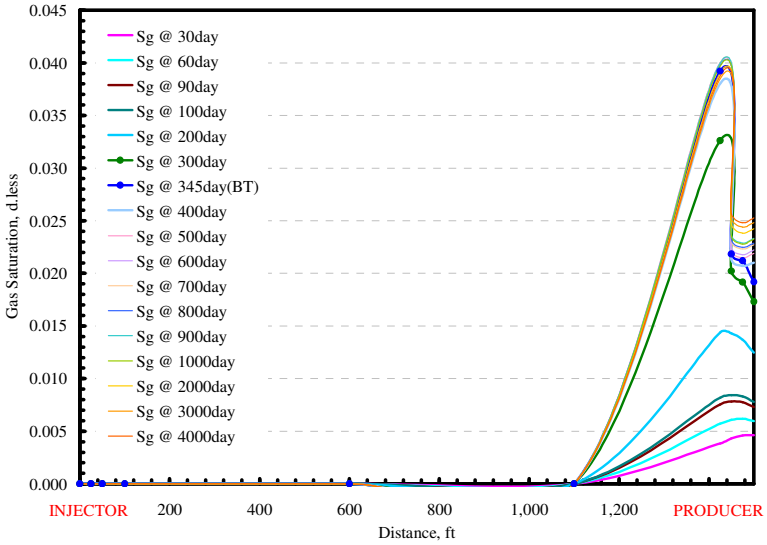

Figure B.2— Gas saturation map showing dissolved gas evolution around the wellbore when C_o=1e-6 1/psi and C_w=1e-6 1/psi.

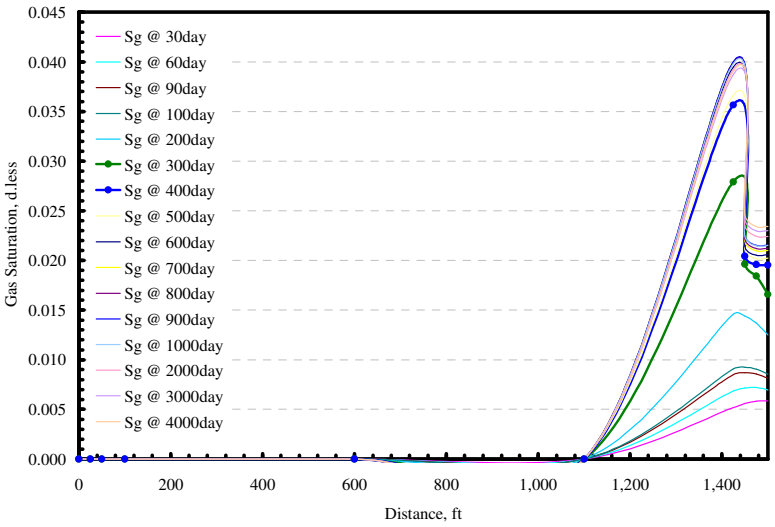

Figure B.3— Gas saturation map showing dissolved gas evolution around the wellbore when C_o=5e-6 1/psi and C_w=1e-6 1/psi.

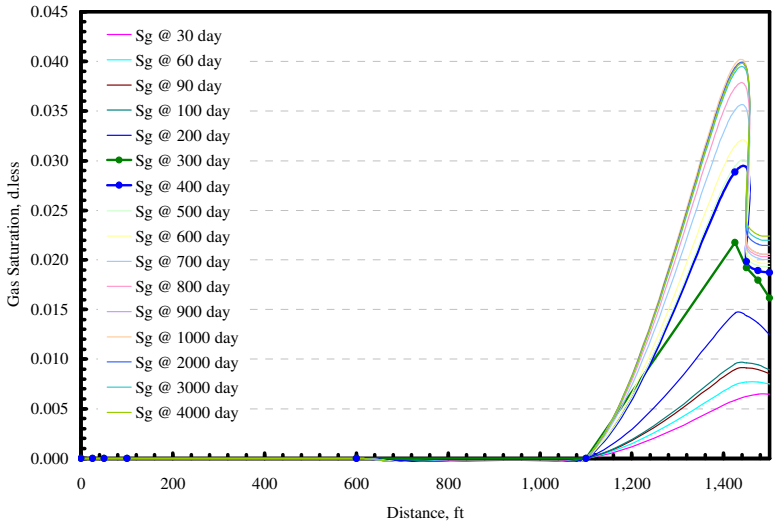

Figure B.4— Gas saturation map showing dissolved gas evolution around the wellbore when C_o=1e-5 1/psi and C_w=1e-6 1/psi.

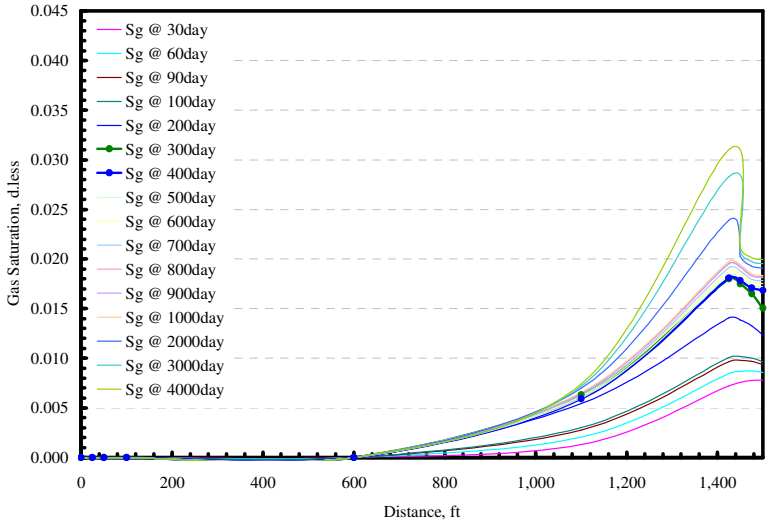

Figure B.5— Gas saturation map showing dissolved gas evolution around the wellbore when C_o=5e-5 1/psi and C_w=1e-6 1/psi.

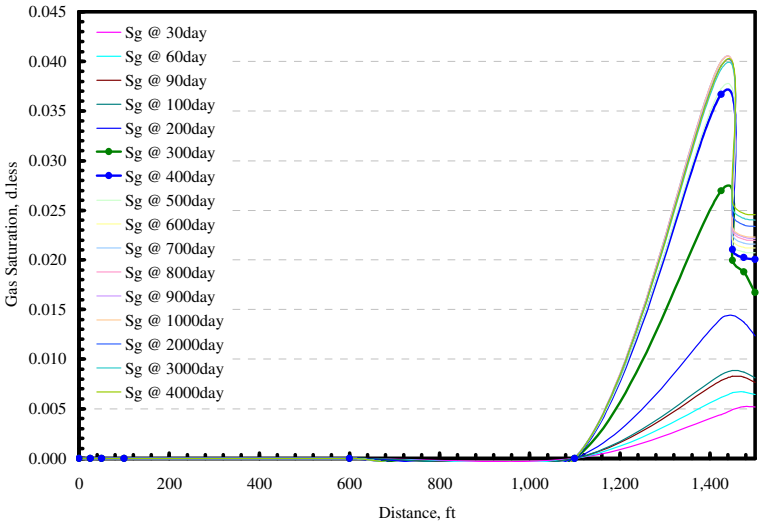

Figure B.6— Gas saturation map showing dissolved gas evolution around the wellbore when C_o=1e-6 1/psi and C_w=1e-5 1/psi.

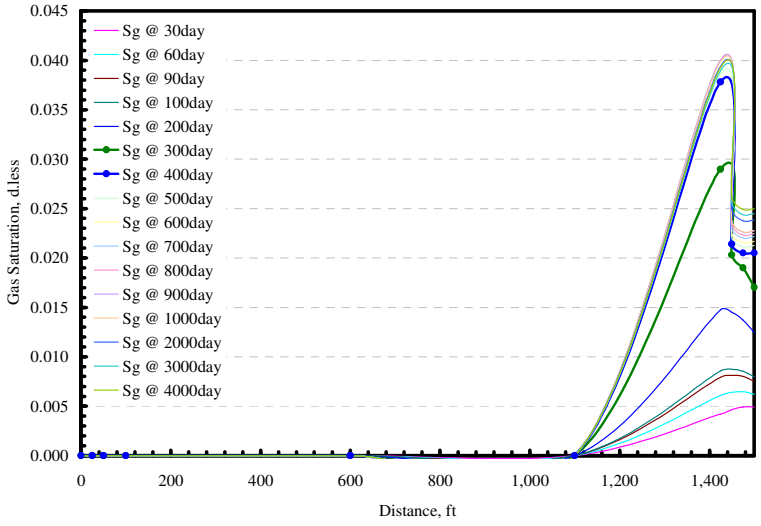

Figure B.7— Gas saturation map showing dissolved gas evolution around the wellbore when C_o=1e-6 1/psi and C_w=5e-6 1/psi.

VITA

Name: Ayse Nazli Demiroren

E-Mail Address: ayse.demiroren@gmail.com

Education: M.S., Petroleum Engineering, Texas A&M University
College Station, USA, 2006

B.S., Petroleum Engineering, Istanbul Technical University
Istanbul, Turkey, 2003